NPS-69-88-008

NAVAL POSTGRADUATE SCHOOL

Monterey, California

Fire Spread in a Three-Dimensional Pressure Vessel with Radiation Exchange and Wall Heat Losses

by

J. Raycraft
M.D. Kelleher
H.Q. Yang
K.Y. Yang

Prepared for: Naval Research Laboratory
Washington, D.C. 20375

Unclassified
SECURITY CLASSIFICATION OF THIS PAGE

REPORT DOCUMENTATION PAGE

1a REPORT SECURITY CLASSIFICATION UNCLASSIFIED	1b RESTRICTIVE MARKINGS
2a SECURITY CLASSIFICATION AUTHORITY	3 DISTRIBUTION AVAILABILITY OF REPORT Approved for public release; distribution unlimited
2b DECLASSIFICATION DOWNGRADING SCHEDULE	
4 PERFORMING ORGANIZATION REPORT NUMBER(S) NPS-69-88-008	5 MONITORING ORGANIZATION REPORT NUMBER(S)
6a NAME OF PERFORMING ORGANIZATION Naval Postgraduate School 6b OFFICE SYMBOL (If applicable) 69Kk	7a NAME OF MONITORING ORGANIZATION Naval Research Laboratory
6c ADDRESS (City, State, and ZIP Code) Monterey, CA 93943-5000	7b ADDRESS (City, State, and ZIP Code) Code 6183 Washington, D.C. 20375
8a NAME OF FUNDING SPONSORING ORGANIZATION Naval Research Laboratory 8b OFFICE SYMBOL (If applicable) Code 6183	9 PROCUREMENT INSTRUMENT IDENTIFICATION NUMBER O & M N, Direct Funding
8c ADDRESS (City, State, and ZIP Code) Washington, D.C. 20375	10 SOURCE OF FUNDING NUMBERS PROGRAM ELEMENT NO. / PROJECT NO. / TASK NO / WORK UNIT ACCESSION NO

11 TITLE (Include Security Classification)
Fire Spread in a Three-Dimensional Pressure Vessel with Radiation Exchange and Heat Losses

12 PERSONAL AUTHOR(S)
J. Raycraft, M.D. Kelleher, H.Q. Yang, and K.T. Yang

13a TYPE OF REPORT	13b TIME COVERED FROM ____ TO ____	14 DATE OF REPORT (Year, Month, Day)	15 PAGE COUNT
		1988 August 1	54

16 SUPPLEMENTARY NOTATION
Prepared in cooperation with the University of Notre Dame

17 COSATI CODES			18 SUBJECT TERMS (Continue on reverse if necessary and identify by block number)
FIELD	GROUP	SUB-GROUP	

19 ABSTRACT (Continue on reverse if necessary and identify by block number)
A three-dimensional differential field model for the spread of fire and smoke, on general orthogonal coordinate systems is developed. The model, which is designed for closed spaces, also includes the physical effects of turbulence, strong buoyancy, full compressibility, pressure rise due to fire loading, surface-surface and surface-flame radiation exchange, and heat losses through the wall. It is based on a control-volume staggered-cell finite-difference approach with primitive variables. Results of numerical calculations based on the field model are compared with test data for a methanol fire in the NRL FIRE I test facility which is in the form of a closed pressure vessel. Reasonable comparisons of the resulting pressure and temperatures at several locations have been obtained. Also shown are the detailed velocity and temperature fields inside the vessel at different time instants after the commencement of the fire.

20 DISTRIBUTION/AVAILABILITY OF ABSTRACT	21 ABSTRACT SECURITY CLASSIFICATION
☑ UNCLASSIFIED/UNLIMITED ☐ SAME AS RPT ☐ DTIC USERS	UNCLASSIFIED
22a NAME OF RESPONSIBLE INDIVIDUAL Prof. M.D. Kelleher	22b TELEPHONE (Include Area Code) (408)646-2530 / 22c OFFICE SYMBOL 69 Kk

DD FORM 1473, 84 MAR 83 APR edition may be used until exhausted
All other editions are obsolete

SECURITY CLASSIFICATION OF THIS PAGE

★ U.S. Government Printing Office: 1986—606-24.

FIRE SPREAD IN A THREE-DIMENSIONAL PRESSURE VESSEL WITH RADIATION EXCHANGE AND WALL HEAT LOSSES

by

Lt. J. Raycraft USN and M. D. Kelleher
Department of Mechanical Engineering
Naval Postgraduate School
Monterey, CA 93943

and

H. Q. Yang and K. T. Yang
Department of Aerospace and Mechanical Engineering
University of Notre Dame
Notre Dame, IN 46556

August 1, 1988

ABSTRACT

In the present study, a three-dimensional differential field model based on general orthogonal coordinate systems is developed. The model, which is essentially designed for closed spaces, also includes the physical effects of turbulence, strong buoyancy, full compressibility, pressure rise due to fire loading, surface-surface and surface-flame radiation exchange, and heat losses through the wall. It is based on a control-volume staggered-cell finite-difference approach with primitive variables. Results of numerical calculations based on the field model are compared with test data for a methanol fire in the NRL FIRE I test facility which is in the form of a closed pressure vessel. Reasonable comparisons of the resulting pressure and temperatures at several locations have been obtained. Also shown are the detailed velocity and temperature fields inside the vessel at different time instants after the commencement of the fire.

TABLE OF CONTENTS

INTRODUCTION

It is now generally recognized that fire hazards in rooms, compartments, corridors, passageways, and other confined spaces can only be minimized and mitigated by a multi-prong approach involving different strategies. Among them is fire modeling which deals with the development of mathematical models which describe the physical and chem-ical processes in the spread of fire in spaces as a function of the ignition source, space geometry, and material content. Once validated by experiments in small-scale laboratory tests and/or full-scale fire tests, these models can be used as computer-based simulation models to determine the effects of the significant parameters on the fire-spread phenomena. The results can then be utilized for developing fire mitigation measures as well as for providing a rational basis for post-fire investigations. One chief advantage of fire modeling is the significantly reduced need for full-scale fire tests which are extremely expensive and time consuming.

Fire models can be categorized as either zone models or field models. Zone models deal with dividing the fire-affected environment or space into distinct regions or zones which can be separately analyzed either empirically or theoretically in terms of input and output information based on mass and energy balances. Examples of such zones include the fire envelope, fire plume, hot gas layer, ceiling jets, wall jet, flow through openings, etc. These input and output quantities from individual zones are then assembled to describe the overall gas dynamic phenomenon of the entire fire environment. In most cases, there results a set of ordinary differential equations in time which are then solved numerically by standard integration algorithms. While the zone models are generally computationally efficient, shortcomings do exist in that the models for some of the zones are not adequately known and quantified, and sometimes there is a question as to exact range of validity of such zone models.

Efforts are now being continued to refine the existing zone models and also to compare with full-scale test data for validation purposes (for example see Rockett et al., 1987).

Field models which are based on the numerical solutions to the governing differential field equations of the conservation of momentum, mass, energy and spices, on the other hand, have not been widely used in the past for fire modeling purposes even though these models are inherently more rational and capable of revealing both the important large-and small-scale phenomena in a given fire-spread problem. The primary reasons are the excessive use of computing resources and degrees of uncertainty in modeling such phenomena as turbulence, combustion and thermal radiation. However, particularly because of the increasing availability of high-performance computers including supercomputers, field models for fire modeling have found increasing use in more recent times. For instance, such models have been developed at the National Bureau of Standards (Baum and Rehm, 1984), Imperial College of London (Bagnaro, Laouisset and Lockwood, 1983), Borehamwood Fire Research Station (Markatos et al., 1982), and the University of Notre Dame (Yang et al., 1984, Yang and Lloyd, 1985), Kou et al., 1986, and Nies, 1986). In view of the different physical and chemical models utilized in each of these field models and the fact that differences also exist in the details of the numerical algorithms involved, there is no way to ascertain the relative accuracies of these models. Comparisons of the numerical results with full-burn tests are scarce, but do exist and are fairly reasonable (Yang et al., 1984; Yang and Lloyd, 1985; Bagnaro et al., 1983, Markatos and Pericleous, 1983). An ultimate assessment of the various field models cannot be made until more validation studies based on full-scale experimental data become available. Additional discussions on fire modeling have been recently given by Stroup (1987).

Despite the above-mentioned uncertainties of the field models, many of the important physical effects can now be accommodated. Those include turbulence (Yang and Liu, 1978; Bagnaro et al., 1983; Marketos and Pericleous, 1983), thermal radiation (Lloyd et al., 1979; Bagnaro et al., 1983; Markatos and Pericleous, 1983); Nies, 1986), combustion (Bagnaro et al., 1983; Markatos and Pericleous, 1983), three-dimensional vented spaces (Bagnaro et al., 1983; Markatos and Pericleous, 1983; Yang and Lloyd, 1985; Nies, 1986), closed-space induced pressure rises (Nies, 1986), and wall losses (Nies, 1986). However, all the above-mentioned field models deal with box-like rectangular spaces or enclosures, and yet, many full-burn facilities have other geometries for which these field models are very difficult to apply. A good example is the facility known as FIRE I located at the Naval Research Laboratory (NRL), which is in the form of a pressure vessel including a central cylindrical body plus two spherical end caps (Alexander et al., 1982). The purpose of this report is to present another field model which is based on a generalized orthogonal coordinate system which still retains the same capabilities in terms of physical models for turbulence, full compressibility, strong buoyancy, surface-to-surface and flame-to-surface radiation, wall losses, and effects of heat addition in a closed space. The rectangular coordinate-system case as given by Nies (1986) becomes a special case of this new field model, and it can be mentioned that the model of Nies (1986) is basically an extension of the original two-dimensional UNDSAFE-II code developed at the University of Notre Dame (Yang and Liu, 1978) for vented rectangular enclosures. Furthermore, this new field model will be demonstrated by presenting a set of numerical results which simulate some experimental data obtained in the NRL FIRE I facility. Finally, several additional capabilities

of this new field model designed to better simulate real fire scenarios will also be delineated.

MATHEMATICAL FORMULATION OF THE FIELD MODEL

As pointed out previously, all field models for the fire-spread phenomena are based on first-principle conservation differential equations for mass, momentum, energy and species. The approach utilized here is similar to that given by Yang et al. (1987a,b), and basically, the governing equations in the Cartesian coordinates are first transformed into those of a generalized orthogonal coordinate system, which are then finite-differenced by the control-volume staggered-cell primitive-variable approach. The flux terms are handled in such a way that the final finite-difference algebraic equations resemble closely those of the Cartesian coordinates. As a result, the computer algorithm for the generalized orthogonal coordinates is no more complex than that for the Cartesian coordinates. In fact, it has recently been shown that the present approach represents a viable alternative to the popular approach of utilizing body-fitted coordinates (Yang et al., 1988). Under the conditions of turbulent compressible flow with buoyancy, the governing equations for the mean quantities in the Cartesian coordinates may be written as follows in the standard tensor forms:

$$\rho_t + (\rho u_i)_{,i} = 0 \tag{1}$$

$$(\rho u_i)_t + (\rho u_i u_j)_{,j} = -P_{,i} - \rho G_i + (\sigma_{ij})_{,j} \tag{2}$$

$$(\rho C_{pm} T)_t + (\rho u_i C_{pm} T)_{,i} = -q_{ci,i} + Q \tag{3}$$

When smoke propagation in the space needs to be considered, an additional equation similar to (3) for the smoke concentration can be added (Yang and Liu, 1978; Raycraft, 1987). It is, however, not shown here, since the smoke field is not considered in the demonstration of this field model, as will be shown later, and in the comparison of the numerical results and the test data. In Eqs. (1), (2) and (3), the physical coordinates are x_i with $i = 1, 2$ and 3, ρ is the mean fluid density, u_i are the mean velocity components in x_i, subscript t signifies the time derivatives, p is the mean static pressure, G_i represents the gravity vector components, T is the mean fluid temperature, and Q represents the source term. It is noted that inside the fire envelope, Q includes both the thermal radiation and combustion heat contributions, and outside the envelope, Q simply vanishes, provided that the gas radiation effects are neglected. Furthermore, the mean isobaric heat capacity c_{pm}, the shear stress tensor σ_{ij}, and the conduction-flux q_{ci} are defined as

$$c_{pm} = \frac{1}{T - T_R} \int_{T_R}^{T} c_p(T)dT \tag{4}$$

$$\sigma_{ij} = \mu_{eff} \left(u_{i,j} + u_{j,i} - 2/3 \ \delta_{ij} u_{k,k}\right) \tag{5}$$

$$q_{ci} = -k_{eff} \ T_{,i} \tag{6}$$

respectively, where T_R is a convenient reference temperature generally taken to be the fluid temperature prior to the commencement of the fire, δ_{ij} is the usual Kronecker delta, and μ_{eff} and k_{eff} are the effective dynamic viscosity

and thermal conductivity, respectively, both accounting for the combined laminar and turbulent contributions. As will be shown later, both μ_{eff} and k_{eff} need to be modeled separately.

In addition, the fluid medium is taken to be a perfect gas, and the perfect gas relation

$$p = \rho RT \tag{7}$$

where R is the fluid gas constant, is not only used to accommodate the compressibility effects, but also needed to account for pressure build-up due to heating from the fire in a constant-volume space. As an approximation, all laminar transport properties, such as c_{pm}, μ and k of the fluid, are considered to be temperature independent and calculated at T_R. This is justifiable because c_{pm} is normally only a weak function of temperature, while μ and k only contribute to a minor degree to the respective effective values due to the much larger turbulent effects expected in the fire phenomena. The initial conditions are simply that there is no motion of the fluid, i.e., $u_i = 0$, and $T = T_R$. The boundary conditions are the usual no-slip conditions at the enclosure interior wall surfaces and that for the temperature field is determined by a heat balance there. When the interior wall is heated up, heat loss occurs through the wall thickness and eventually to the environment from the exterior wall. In the present study, such wall losses are accommmodated by transient conduction through the wall and then by combined convection and radiation at the outer surface by means of a constant coefficient of heat transfer. Since the wall thickness is always small compared to the characteristic length along the wall, a one-dimensional conduction analysis should be sufficient. Thus, for conduction through the wall thickness, we may write

$$\rho_s c_s T_{st} = (k_s T_s)_{,n} \tag{8}$$

where the subscript refers to the wall material, and n is the outward normal coordinate, together with the boundary conditions:

$$n = 0 \qquad q_r - k_{eff} \frac{\partial T}{\partial n} = -k_s \frac{\partial T_s}{\partial n} \tag{9}$$

$$n = L_w \qquad -k_s \frac{\partial T_s}{\partial n} = h(T - Te) \tag{10}$$

where $n = 0$ is at the inner surface, L_w is the wall thickness, h is the coefficient of heat transfer at the outer surface, T_e is the environment temperatures and q_r is the thermal radiation flux arriving at the surface from the enclosure interior. As pointed out previously, h is taken to be a constant, depending on the wind conditions outside. Before Eqs. (1), (2), (3) and (8) can be solved simultaneously, additional turbulence and thermal radiation models must be introduced, and these models will be given in a later section.

Now the above governing equations in x_i are ready to be transferred into those of a generalized orthogonal coordinate system given by the coordinates θ^i. The two coordinate systems are related by means of the scale factors h_i in the direction θ^i given by

$$h_i = (\vec{g}_i \cdot \vec{g}_i)^{1/2} = \left(\frac{\partial x_j}{\partial \theta^i} \cdot \frac{\partial x_j}{\partial \theta^i}\right)^{1/2} \tag{11}$$

where $\vec{g}_i$ is the base vector. One of the special properties of the orthogonal coordinates is that these base vectors are orthogonal so that the covariant and contravariant metric tensors satisfy the following conditions

$$g_{ij} = \vec{g}_i \cdot \vec{g}_j = \delta_{ij} h_i h_j \tag{12}$$

$$g^{ij} = \frac{\delta_{ij}}{h_i h_j} \tag{13}$$

resulting in a diagonalized metric tensor, where g is the determinant of g_{ij}, or

$$g = |g_{ij}| = h_1^2 h_2^2 h_3^2 \tag{14}$$

With the above orthogonal properties, transformations of Eqs. (1), (2) and (3) in the x_i system lead to the following respective equations in the θ^i system:

$$\rho_t + \frac{1}{g^{1/2}} \frac{\partial}{\partial \theta^i}(g^{1/2} \rho u^i / h_i) = 0 \tag{15}$$

$$(\rho u^i)_t + \frac{1}{g^{1/2}} \frac{\partial}{\partial \theta^j}(g^{1/2} u^i u^j / h_j) = - P_{,i}/h_i + \rho G^i + \frac{1}{g^{1/2}} \frac{\partial}{\partial \theta^j}(g^{1/2} \sigma_i^j / h_j)$$

$$- \frac{1}{h_i h_j} \frac{\partial h_i}{\partial \theta^j}(\rho u^i u^j - \sigma_i^j) + \frac{1}{h_i h_j} \frac{\partial h_j}{\partial \theta^i}(\rho u^j u^i - \sigma_j^j) \tag{16}$$

$$(\rho C_{pm} T)_t + \frac{1}{g^{1/2}} \frac{\partial}{\partial \theta^i} (g^{1/2} \rho C_{pm} u^i T/h_i)$$

$$= \frac{1}{g^{1/2}} \frac{\partial}{\partial \theta^i} (g^{1/2} kT_{,i}/h_i^2) + Q \tag{17}$$

where

$$\sigma_i^j = \mu_{eff} \left[\frac{h_j}{h_i} \frac{\partial}{\partial \theta^i} \left(\frac{u^j}{h_j}\right) + \frac{h_i}{h_j} \frac{\partial}{\partial \theta^j} \left(\frac{u^i}{h_i}\right) + \frac{\delta_{ij}}{h_i h_j} \frac{\partial q_{ii}}{\partial \theta^m} \frac{u^m}{h_m}\right.$$

$$\left. - \frac{2}{3} \frac{\delta_{ij}}{g^{1/2}} \frac{\partial}{\partial \theta^m} \left(g^{1/2} \frac{u^m}{h_m}\right)\right] \tag{18}$$

The above conservation equations are clearly valid for any orthogonal coordinate systems. In particular, $h_1 = h_2 = h_3 = 1$ for the Cartesian coordinates; $h_1 = r = \theta^2$, $h_2 = h_3 = 1$ for the cylindrical coordinate system where r is the radial variable; and $h_1 = r\sin\phi = \theta^2 \sin\theta^3$, $h_2 = 1$, $h_3 = r = \theta^2$ for the spherical coordinates, where ϕ is the polar angle. The boundary and initial conditions need no further transformation. In addition, in view of the relatively thin wall thickness, one-dimensional conduction is still valid and therefore, Eqs. (8), (9) and (10) remain the same.

As pointed out previously, before the governing equations (15), (16), (17) and (8) can be solved, physical models for the radiation exchange in the enclosure and for the turbulence field are still needed. Since the radiation exchange depends on the specific geometry of the enclosed space, the radiation model will be described later after the geometry of the NRL FIRE I test facility

is introduced. However, a turbulence model utilized in the present study can be given here, again in terms of an arbitrary orthogonal coordinate system. This model is based on a mixing-length formulation originally developed for two-dimensional recirculating flows (Nee and Liu, 1978), and has been extended to three-dimensional flows with good success (Yang and Lloyd, 1985). In terms of the orthogonal coordinate system, the equation for the effective viscosity according to this model can be written as

$$\frac{\mu_{eff}}{\mu_R} = 1 + \frac{[(\frac{1}{h_j}\frac{\partial u^i}{\partial \theta^j})^2(1-\delta_i^j)]^{1/2}(\frac{\ell}{H})^2}{2+\frac{Ri}{Pr_t}} \tag{19}$$

where μ_R is the laminar viscosity at T_R, Pr_t is the turbulent Prandtl number taken to be unity, and R_i is the gradient Richardson number given by

$$Ri = \frac{H}{U_R^2}\frac{(\frac{\partial T}{\partial n})\vec{n}\cdot\vec{g}}{[(\frac{\partial u^1}{\partial n})\vec{n}\cdot\vec{g}]^2+[(\frac{\partial u^2}{\partial n})\vec{n}\cdot\vec{g}]^2+[(\frac{\partial u^3}{\partial n})\vec{n}\cdot\vec{g}]^2} \tag{20}$$

where U_R is a reference velocity, and $\vec{n}$ is a unit vector in the negative gravity direction. In addition, the mixing length ℓ normalized with the enclosure height H can be written as:

$$\frac{\ell}{H} = K\left\{\frac{(u^i u^i)^{1/2}}{[\sum_{i,j}(\frac{1}{h_j}\frac{\partial u^i}{\partial \theta^j})^2]^{1/2}} + \frac{[\sum_{i,j}(\frac{1}{h_j}\frac{\partial u^i}{\partial \theta^j})^2]^{1/2}}{[\sum_{i,j}(\frac{1}{h_i h_j}\frac{\partial^2 u^1}{\partial \theta^i \partial \theta^j})^2]^{1/2}}\right\} \tag{21}$$

where K is a constant, normally taken to be 0.2. Finally, the effective conductivity k_{eff} is given by

$$\frac{k_{eff}}{k_R} = \frac{1}{Pr} + \frac{1}{Pr_t}\frac{\mu_{eff}}{\mu_R} \tag{22}$$

where k_R is the molecular thermal conductivity at T_R, and Pr is the corresponding laminar Prandtl number.

NUMERICAL FINITE-DIFFERENCE CALCULATIONS

In the present study, the governing equations (15), (16) and (17) in the generalized orthogonal coordinates are solved by means of the primitive-variable staggered control-volume finite-difference approach. As recently pointed out by Yang et al. (1987b, 1988), one major advantage of utilizing the fully transformed equations is that by judiciously choosing new definitions of flux and source quantities, the final finite-difference equations appear very much like those for the well-known Cartesian-coordinate cases, and hence can be handled in a routine manner for their solutions. That this is the case can be illustrated as follows:

For a control volume given by $\Delta V = \sqrt{g}\,\Delta\theta^1\Delta\theta^2\Delta\theta^3$, where Δ indicates a step size, the mom entum equation (16) for u^1, after integrated over the staggered control volume surrounding a grid point P, becomes

$$\Delta V(\rho u^1)_t + Me^{11}Ae - Mw^{11}Aw + Mn^{12}An$$

$$- Ms^{12}As + M_f{}^{13}A_f - M_b{}^{13}A_b = S \tag{23}$$

where the areas A are given by

$$A_{e,w} = (h_2 \Delta\theta^2 h_3 \Delta\theta^3)_{e,w}$$
$$A_{f,b} = (h_1 \Delta\theta^1 h_2 \Delta\theta^2)_{f,b} \qquad (24)$$
$$A_{n,s} = (h_3 \Delta\theta^3 h_1 \Delta\theta^1)_{n,s}$$

and M^{ij} is the total momentum flux along the θ^j direction for the velocity component u^i due to convection and diffusion. The subscripts e, w, n, s, f and b denote the east, west, north, south, front and back boundaries one-half cell size away from the point P, respectively. More specifically,

$$M^{ij} = (\rho u^i u^j - \sigma_i^j) \qquad (25)$$

$$S = -P_e A_e + P_w A_w + \rho G^1 \Delta V - M_p^{12}(A_n - A_s)$$

$$- M_p^{13}(A_f - A_b) + (M_p^{22} + M_p^{33})(A_e - A_w) \qquad (26)$$

Here the idea of Raithby et al. (1986) of using a stress-flux formulation is utilized, and the momentum flux is then split into

$$M^{ij} = \hat{M}^{ij} + (\hat{\sigma}_i^j - \sigma_i^j) \qquad (27)$$

where

$$\hat{\sigma}_i^j = \mu_{eff} \left[h_j \left(\frac{\partial u^i}{\partial \theta^j}\right)\right] \qquad (28)$$

$$\hat{M}^{ij} = \rho u^i u^j - \hat{\sigma}_i^j \qquad (29)$$

As a result, Eq. (23) now becomes

$$\Delta V\,(\rho u)_t + \hat{M}^{11}_e A_e - \hat{M}^{11}_w A_w + \hat{M}^{12}_n A_n - \hat{M}^{12}_s A_s + \hat{M}^{13}_f A_f - \hat{M}^{13}_b A_b = \hat{S} \tag{30}$$

where

$$\hat{S} = S - (\hat{\sigma}^1_1 - \sigma^1_1)_e A_e + (\hat{\sigma}^1_1 - \sigma^1_1)_w A_w - (\hat{\sigma}^2_1 - \sigma^2_1)_n A_n + (\hat{\sigma}^2_1 - \sigma^2_1)_s A_s - (\hat{\sigma}^3_1 - \sigma^3_1)_f A_f + (\hat{\sigma}^3_1 - \sigma^3_1)_b A_b \tag{31}$$

Here the stresses σ^j_i are evaluated from the information of the prior iteration, and the source term is known at the present iteration. Once these are properly evaluated, Eq. (30) becomes identical in form to that for the Cartesian coordinates. Further approximations to $\hat{M}^{ij}$ can be made. Basically, the convective terms are approximated by the QUICK scheme of Leonard (1983), extended to three-dimensional cases, and the diffusion terms are by central differences. The details have been given by Raycraft (1987), and hence will not be repeated here.

The treatment of the energy equation is very similar. For example, a total heat flux J^i, which includes both convection and conduction, is introduced as

$$J^i = \rho\, c_{pm}\, T - kT_{,i}/hi \tag{32}$$

The corresponding finite-difference equation for the energy equation (17) then becomes

$$(\rho\, c_{pm}\, T)_t\, \Delta V + Je^1 Ae - Jw^1 Aw + Jn^2 An$$

$$- Js^2 As + J_f{}^3 A_f - J_b{}^3 A_b = S_T \qquad (33)$$

where the source S_T also includes Q and the solution procedure is the same as that for the momentum equations.

In addition, it is noted that for a closed enclosure, any energy addition to the gas due to the fire tends to raise the pressure in the enclosure in view of the constant volume. Consequently, a time-dependent global pressure correction is needed to determine this rise, in addition to the local pressure correction in the primitive-variable control-volume procedure, which only depends on the local velocity variations. For this purpose, the technique based on the perfect gas relation as developed by Nicolette et al. (1985) is utilized in the present study, and this technique has also been described by Raycraft (1987).

NRL FIRE I TEST FACILITY AND RADIATION MODEL

As pointed out previously, the validation of the field model developed in the present study is based on test data obtained in the Naval Research Laboratory (NRL) FIRE I full-scale test facility (Alexander et al., 1982). As shown schematically in Fig. 1, the facility has a cylindrical midsection with a radius of 9.6 feet (2.93m) and a length of 27.4 feet (8.352m) and hemispherical end caps. Thus, it is in the form of a pressure vessel having a total volume of 11,639 cubic feet (324m^3). The instrumentation consists of pressure transducers, thermocouples, and radiometers. There is also capability to measure smoke obscuration levels, gas composition and humidity. The use of circulation fans can also be included in a test to determine the effect of ventilation.

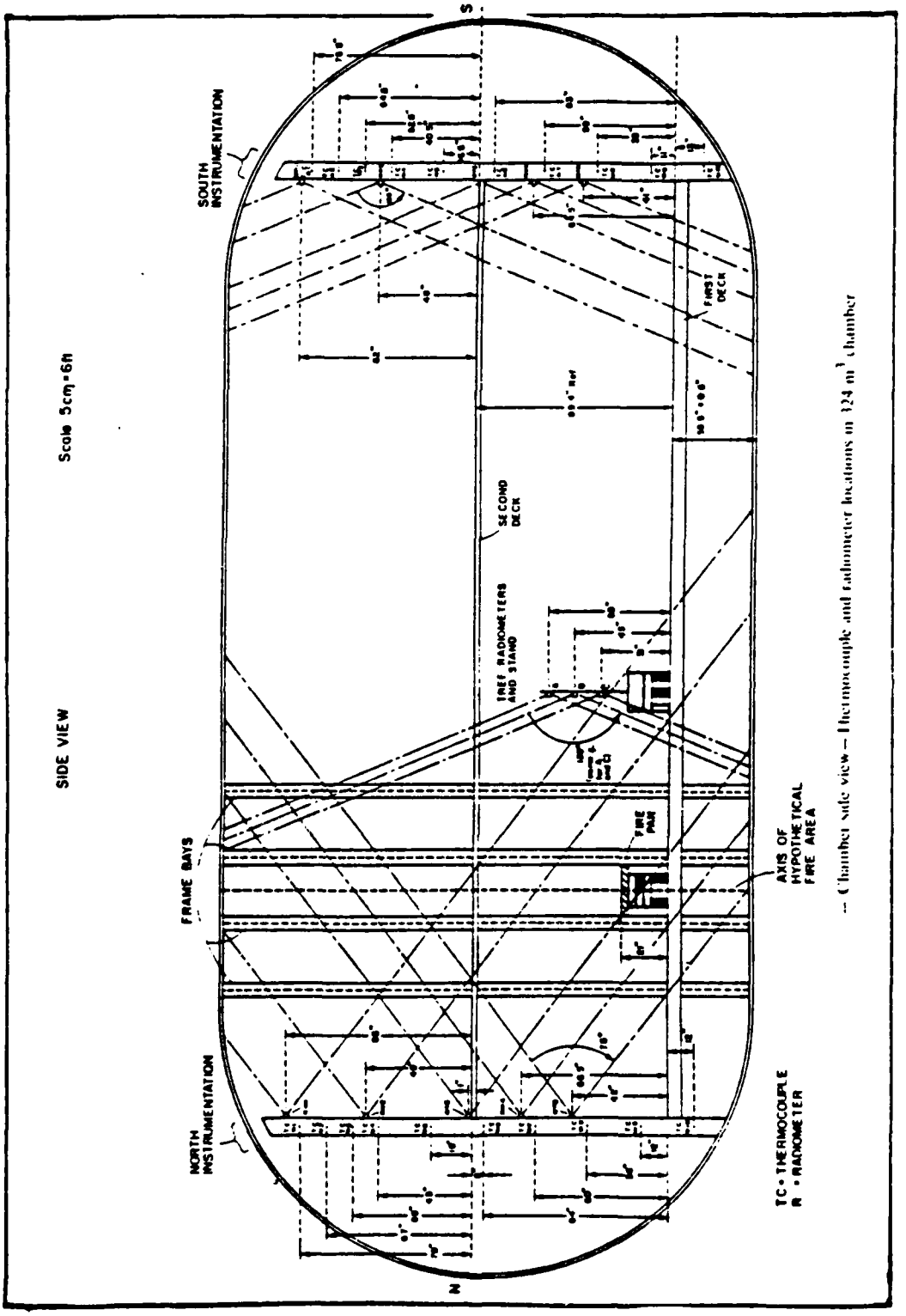

-- Chamber side view -- thermocouple and radiometer locations in 124 m^3 chamber

Figure 1 Side View of Fire I with Sensor Locations

Pressure transducers are located at the north and south ends of the test chamber, while the temperatures are monitored with thermocouple arrays located inside the spherical end caps as shown in Fig. 1. These are chromel-alumel thermocouples with diameters of 0.12 mm and have ceramic insulation enclosed in 304 stainless steel jackets 1.0 mm in diameter. As will be shown later, these temperature readings provide the data for comparison with the numerical calculations based on the field model.

In the field of fire modeling, the importance of thermal radiation contribution to the energy transfer and turbulent buoyant flow processes involved is generally well recognized. However, accommodation of the radiation effects in fire models is always difficult and requires solutions to the radiative transfer equation for complex geometries and nongray-gas, nonhomogeneous, and nonisothermal behaviors (Yang, 1986). The presence of soot and smoke further complicates the situation, even though some simplification here is possible. Therefore, any reasonable simplification in including the radiation effects is desirable. In the present study, only surface-surface and flame-surface radiation exchange is included in the field model. In other words, the gas outside the flame envelope is taken to be transparent. In addition, the flame is considered to be represented by an equivalent gray surface which exchanges radiation with all other surfaces in the enclosure. This simplification is deemed reasonable, since it is known that the effects of participating gases in an enclosure is largely to equalize the gas temperatures, and the radiation exchange is in general dominated by surface-surface interactions (Chang et al., 1983). Under this simplification, the radiation heat transfer can be readily calculated by any one of the well-known enclosure procedures (Sparrow and

Cess, 1978; Siegel and Howell, 1981). In the present study, the radiation calculations are based on the net radiosity method which is particularly suited for gray surfaces. The radiosity B_i at a surface i can be written as

$$B_i = \epsilon_i \sigma T_i^4 + (1 - \epsilon_i) \sum_{j=1}^{N} B_j F_{ij} \tag{34}$$

where ϵ is the emissivity, and F_{ij} is the direct view factor from surface i to surface j. The index N denotes the total number of surfaces in the enclosure, including that of the flame. The above equation results in N linear, inhomogeneous, algebraic equations for the N unknown radiosities. By solving the simultaneous equations, usually by matrix inversions, B_i can be found, and the radiation heat flux at surface i can then be readily calculated from

$$q_{ri} = \frac{\epsilon_i}{1 - \epsilon_i} (\sigma T_i^4 - B_i) \tag{35}$$

which, for all enclosure interior surface elements, becomes part of the thermal boundary conditions in accordance with Eq. (9). This method of calculating q_{ri} can be further simplified by obtaining a direct relation between q_{ri} and the temperatures T_i so that matrix manipulations can be kept at a minimum. Eq. (34) can be rewritten as

$$\sum_{j=1}^{N} X_{ij} B_j = \sigma T_i^4 \tag{36}$$

where

$$X_{ij} = \frac{\delta_{ij} - (1 - \epsilon_i) F_{ij}}{\epsilon_i} \tag{37}$$

which, in a matrix form, becomes

$$[X] \langle B \rangle = \sigma \langle T^4 \rangle \tag{38}$$

By inverting the coefficient matrix [X], we obtain for the radiosity

$$\langle B \rangle = \sigma [X]^{-1} \langle T^4 \rangle \tag{39}$$

Then in accordance with Eq. (35), we finally have

$$q_{ri} = \sum_{j=1}^{N} G_{ij} \sigma T_j^4 \tag{40}$$

where

$$G_i = \frac{\epsilon_i}{1 - \epsilon_i} (\delta_{ij} - X_{ij}^{-1}) \tag{41}$$

Here X_{ij}^{-1} only depends on the emissivities which are taken to be constants, and consequently, together with G_{ij}, can be calculated once for all in a given problem.

It is thus clearly seen that the radiation model utilized in the present study essentially reduces to a problem of determining all the appropriate view factors F_{ij}. To be consistent to the finite-difference calculations for the buoyant flow in the enclosure, in which each interior surface cell has a temperature which depends on time, these surface cells can also be conveniently used as surfaces i for radiation. Consequently, the determination of the view factors does not require any surface integration, and they can be calculated directly from the definition

$$A_i F_{ij} = \frac{\cos\beta_i \cos\beta_j}{\pi R^2} A_i A_j \qquad (42)$$

where β is the angle between the normal of the surface and R, the line connecting A_i and A_j. Since F_{ij} depends strongly on the geometry of the enclosure, no generic forms can be written in terms of the generalized orthogonala coordinates, and this is the very reason that the radiation model cannot be introduced until the geometry is specified.

For the geometry of FIRE I, the view factors F_{ij} depend on such surface cell pairs as internal cylindrical to cylindrical, cylindrical to hemispherical, and hemispherical to hemispherical surfaces. For the last case, surfaces i and j may also be located on different end caps. Surprisingly, not all such view factors are known in the literature (Siegel and Howell, 1981). As a result, these view factors have been derived directly from the FIRE I geometry. They have been given by Raycraft (1987) and there is no need to repeat them here. Furthermore, the view factors associated with the flame must be treated somewhat differently, and this will be given in the following section.

RESULTS OF NUMERICAL CALCULATIONS AND DISCUSSIONS

Detailed numerical calculations based on the field model have been carried out for the NRL FIRE I facility geometry so that the results can be compared directly with the test data. One set of test data for burning methanol inside the FIRE I tank is chosen for this purpose. For this burn test, the tank is essentially empty and the fuel pan is located at 23.1 feet (7.041m) from either end cap and elevated 3.21 feet (0.978m) from the bottom. The initial temperature and pressure are at 35.6°C and 1 atm., respectively. Shown in Fig. 2

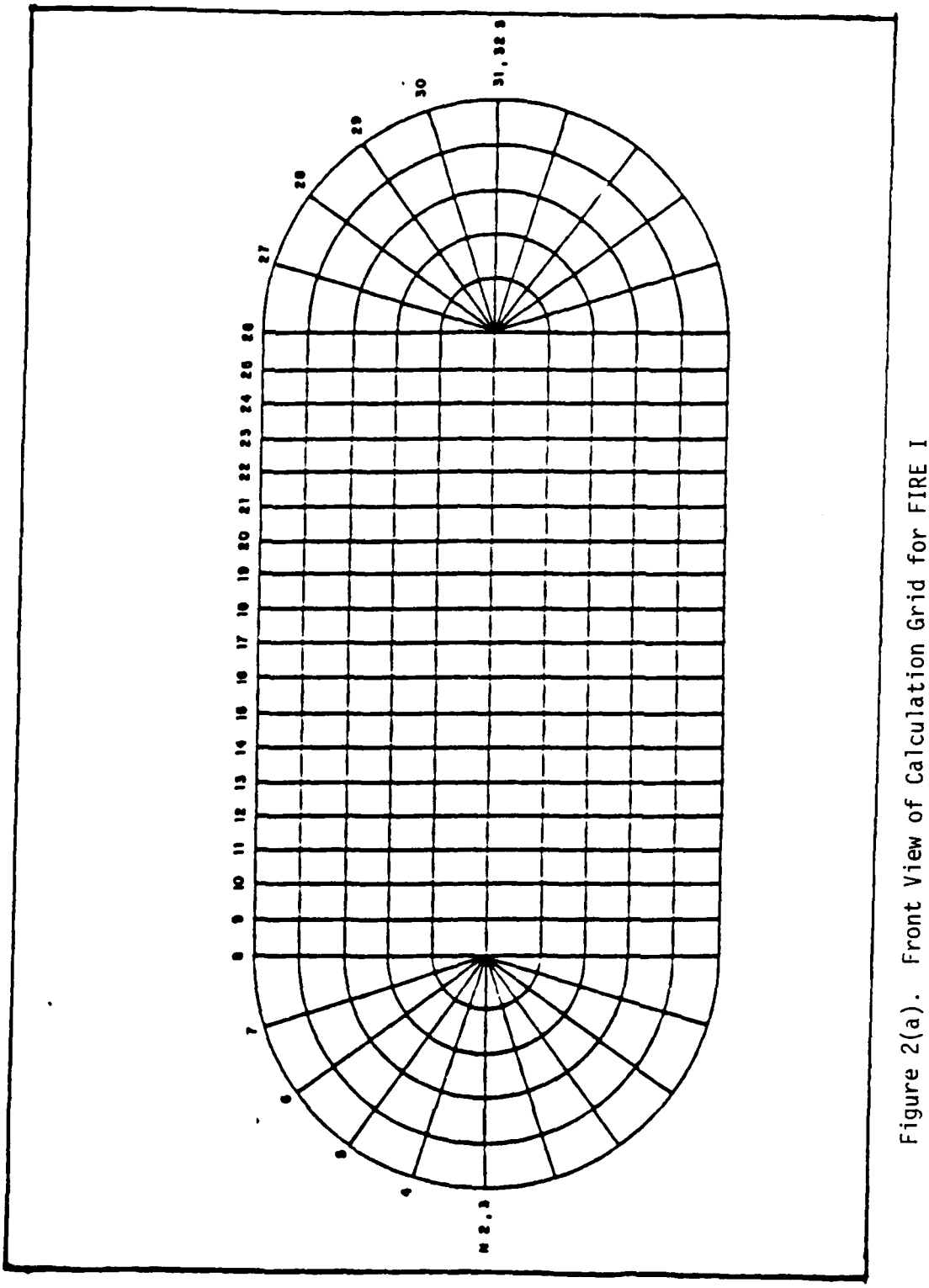

Figure 2(a). Front View of Calculation Grid for FIRE I

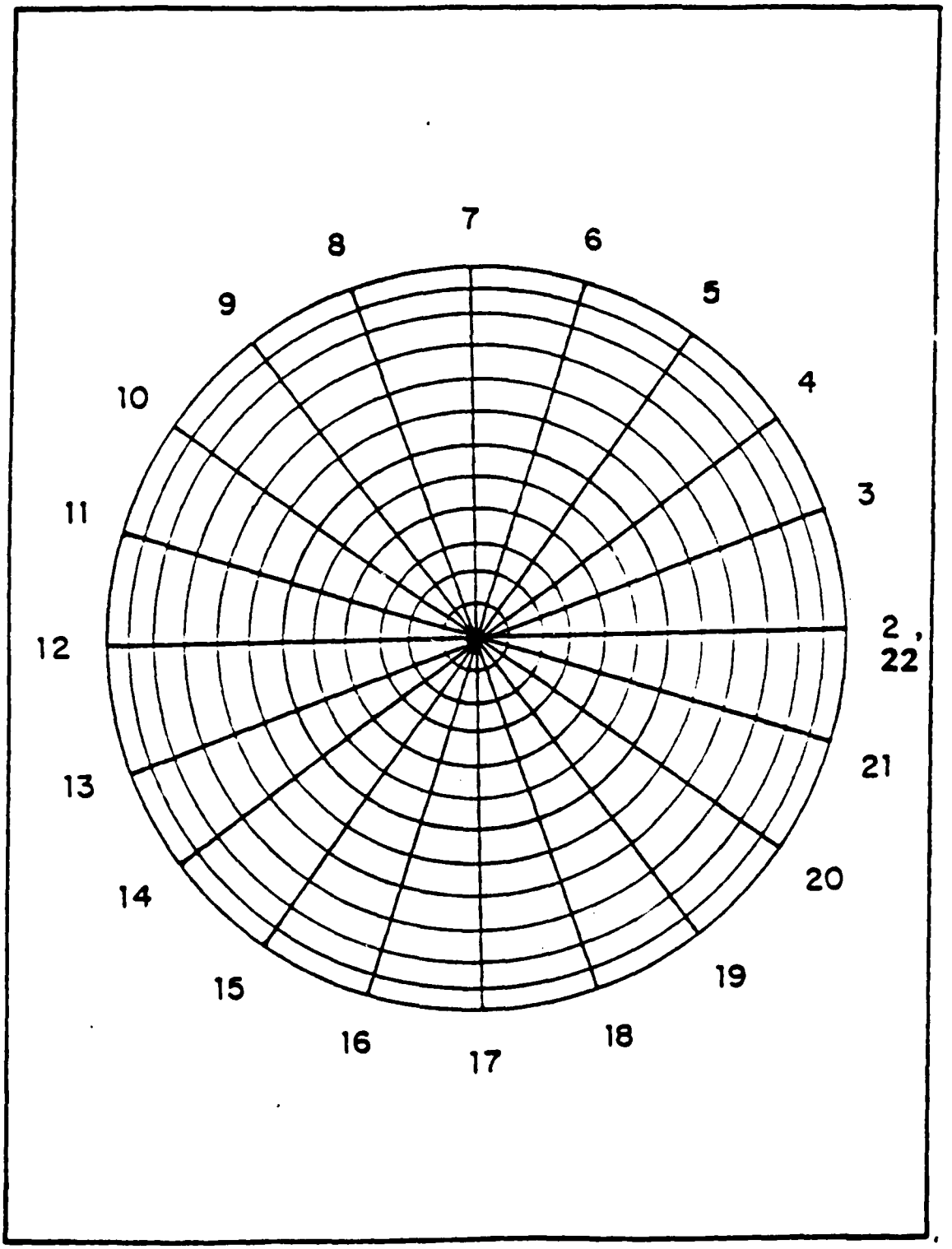

Figure 2(b). End View of Calculation Grid for FIRE I

is the grid system utilized in the computations. As seen, there are 20 segments in the circumferential direction, 12 radial segments representing the interior of the tank, and 18 segments along the cylindrical midsection, for a total of 6,720 interior cells. Also, in order to avoid calculation difficulties surrounding the line of zero radius, a row of cells is added to preserve the direction of the velocity vectors (Yang et al., 1987b). The thickness of the wall is 0.375 in (0.95 cm), and occupies one single cell segment. Consequently, the entire interior surface of the tank has 560 surface cells which all exchange radiation with the flame and also with each other, and there are also 560 cells for conduction through the wall thickness. Furthermore, similar to that in the UNDSAFE-II field model (Yang and Liu, 1978), the flame is modeled as a volumetric heat source, and in the present calculations, the entire heat release rate in the flame is taken to be distributed uniformly over 19 cells above the fuel pan. Thus, radiation heat transfer calcula-tions involve altogether 579 surfaces. The numerical calculations also require several physical data relative to the wall properties and external boundary conditions. In addition to the wall thickness given previously, the specific heat, thermal conductivity, and density of the metallic wall (ASTM-285 Grade C steel) are taken to be 0.1 B/(lbF) (0.42 kJ/kgK), 25 B/hr.ft.F(43.27 W/mK), and 487 lb/ft^3 (7,801 kg/m^3), respectively. There is also convection and radiation heat transfer occurring at the tank exterior surface, and the corresponding coefficient of heat transfer is taken to be a constant of 15 B/hr.ft^{2}F (85.169 W/m^{2}K). This coefficient can be adjusted in the computations, if needed. The time increment is essentially determined by numerical stability requirement.

The driving force in the physical problem is the heat release rate from the fire. Since in the present model the flame is taken to be a volumetric heat source, the unsteady heat release rate must be treated as an input. Normally, such data can be obtained from the fuel depletion rate and the heating value of the fuel. Unfortunately, because of instrumentation error during the methanol fire test, the fuel depletion rate data were also in error, and consequently the heat release rate must be determined in an indirect way. Since the static pressure in the tank during the fire test was recorded, and in a constant volume heat addition process, the heat added is directly proportional to the rate of rising static pressure, an estimate of the heat release rate can be obtained from the recorded pressure data. In an attempt to generate the unsteady heat release rate in this way automatically on the computer. a pressure-tracking routine based on feedback control and the field model has been developed (Nies, 1986; Raycraft, 1987). The result is shown in Fig. 3. Even though the routine is performing well insofar as the pressure level is concerned, the resulting heat release rate, which is sensitive to the time derivative of the pressure, oscillates with large variations leading also to large variations in the temperature field in the tank. This heat release rate from the pressure-tracking is given in Fig. 4. Since such large variations of the heat release rate are not expected in the fire test, it is reasonable to use a curve-fitted variation as the input to the field model calculations, as also shown in Fig. 4. In order to demonstrate that such a curve-fitted heat release rate variation is a reasonable approximation to the real data, the calculated pressure rise is also given in Fig. 3, and it is seen that it does follow the experimental curve rather well. Detailed intermediate results based on pressure tracking can be found in the thesis of Raycraft (1987).

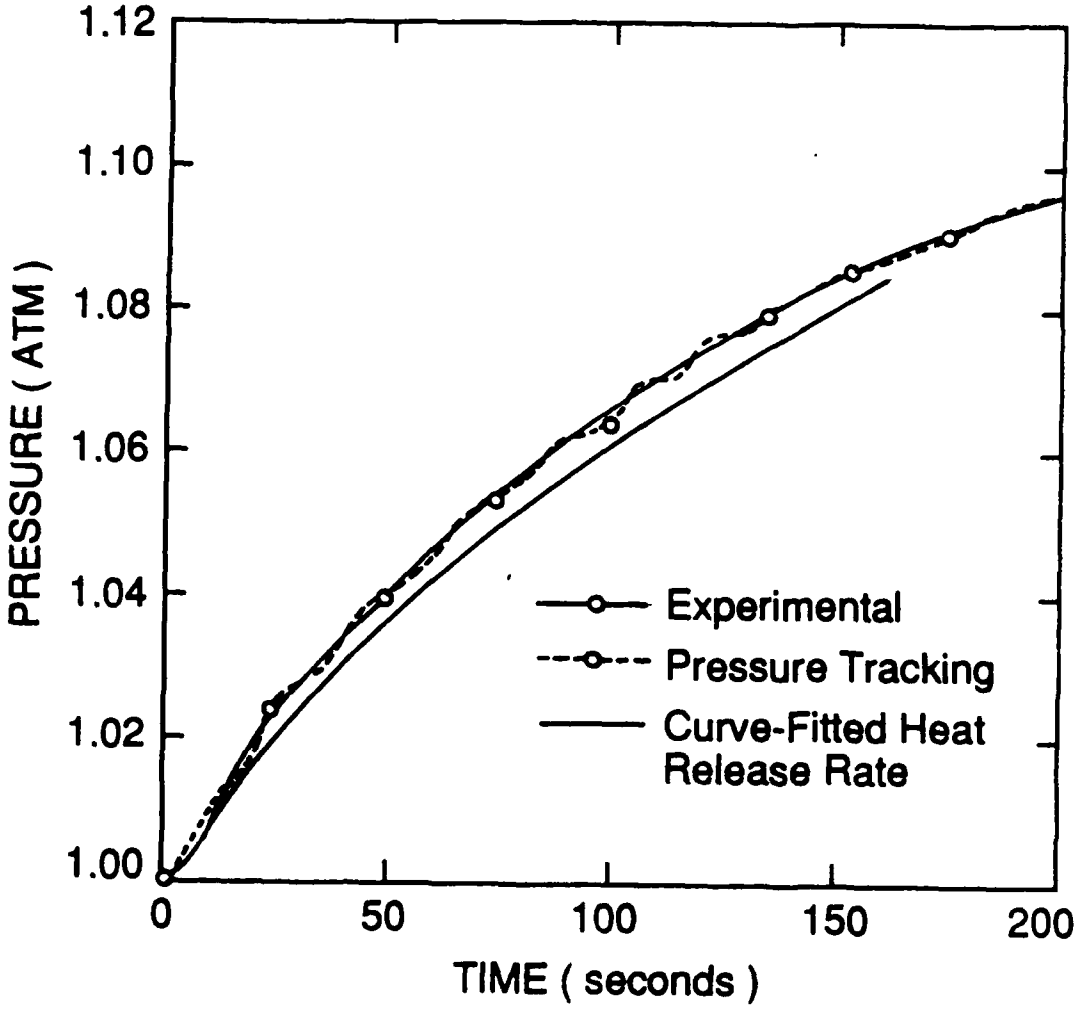

Figure 3. Pressure History After Commencement of Fire

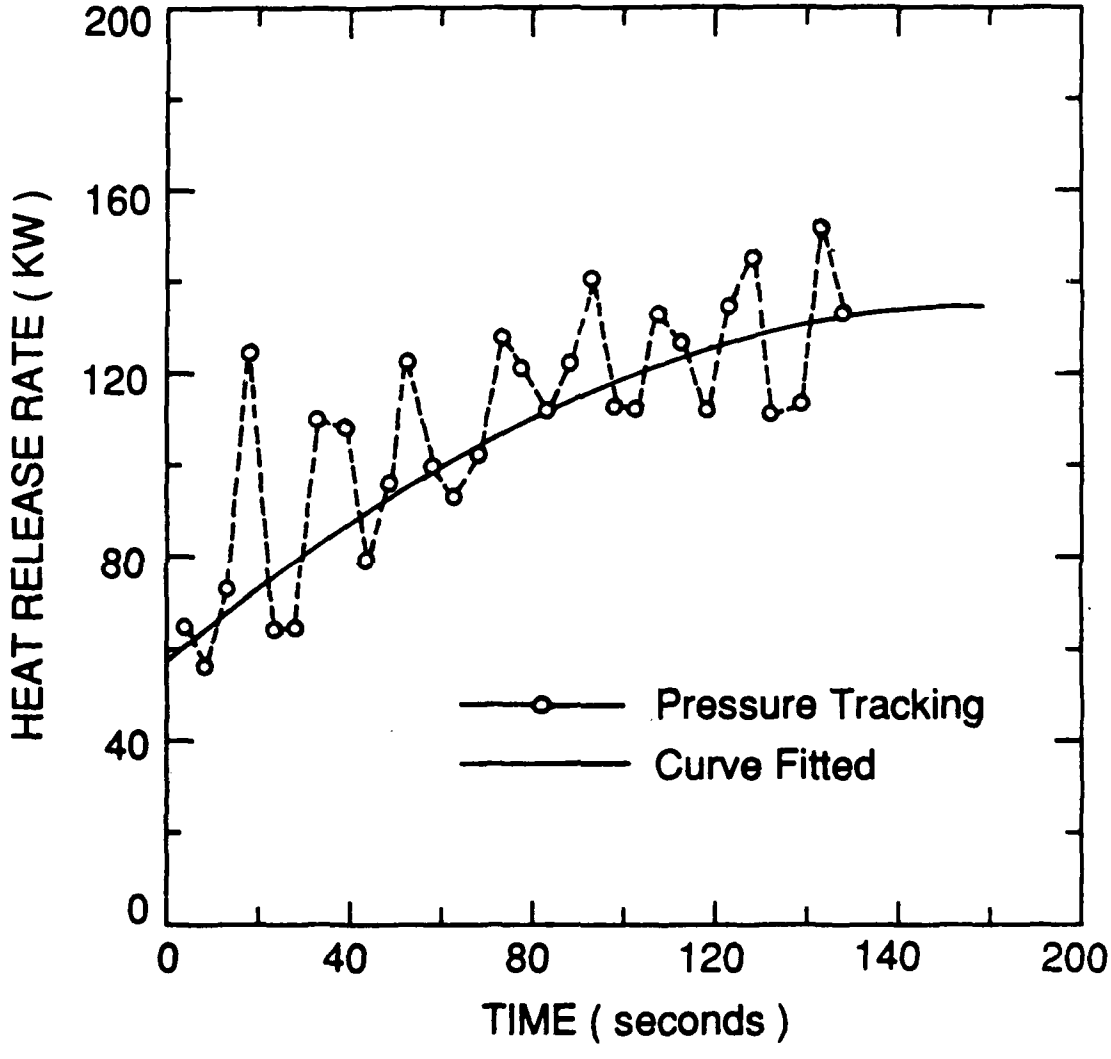

Figure 4. Input Heat Release Rate

A more important result of the numerical computations is to compare the temperatures at the various thermocouple locations with those from the test. The thermocouples are all mounted on vertical racks in the two end-cap regions close to the edges of the cylindrical midsection (Fig. 1). The three thermocouples, 1, 2 and 4, are located in the south hemispherical end cap, and the readings there are compared with the numerical results. Thermocouple 1 is located 79 inches (2.01 m) above the midplane of the tank. Thermocouple 2 is one foot (0.305 m) below thermocouple 1, and thermocouple 4 is at two feet (0.61 m) below thermocouple 2. The thermocouple 3 was defective during the test, and hence comparisons there are not made. Figs. 5, 6 and 7 show the temperature variations at thermocouples 1, 2 and 4 locations, respectively, as compared to those from the test, which represent smoothed mean temperatures. The agreement is reasonable at the two lower thermocouple locations with maximum deviations of less than 10°C. However, the calculations definitely overpredict the temperatures at the thermocouple 1 location by a maximum of about 30°C. Several possible reasons may be responsible. One is that since the thermocouple 1 location is closest to the tank wall, its temperature is most affected by the boundary condition at the tank exterior surface in terms of outside ambient temperature and the coefficient of heat transfer, both of which have been estimated for calculation purposes. Another possible reason is that in the model, the heat release rate is taken to be uniformly distributed. In reality, considerable vertical nonuniformity may result from the combustion process in the flame. If more heat is released in the lower part of the flame, more heat would be radiated away there so that the thermal plume would attain a lower temperature, resulting also in lower temperatures at the thermocouple 1 location. A third

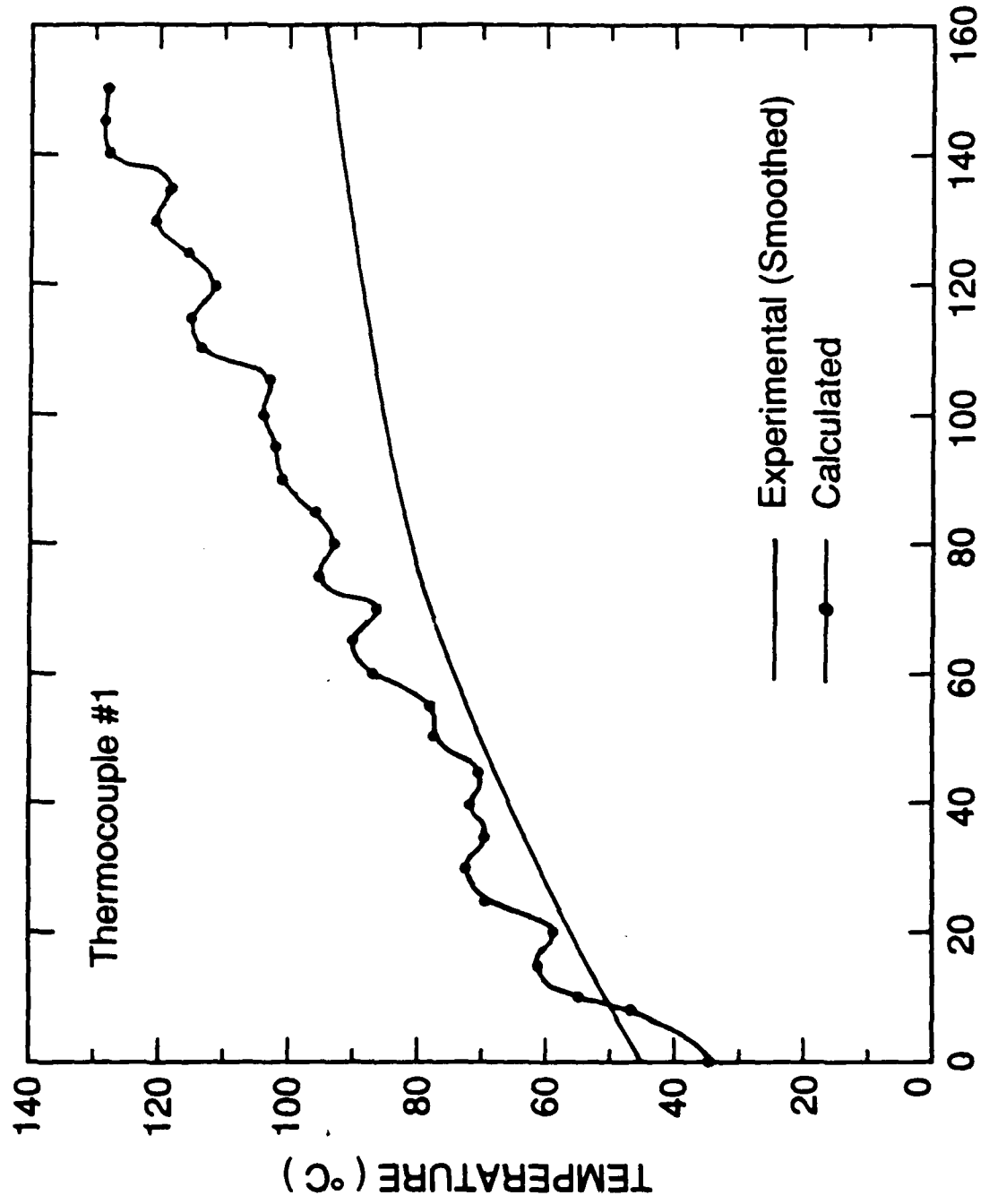

Figure 5. Temperature Comparison at Thermocouple #1 Location

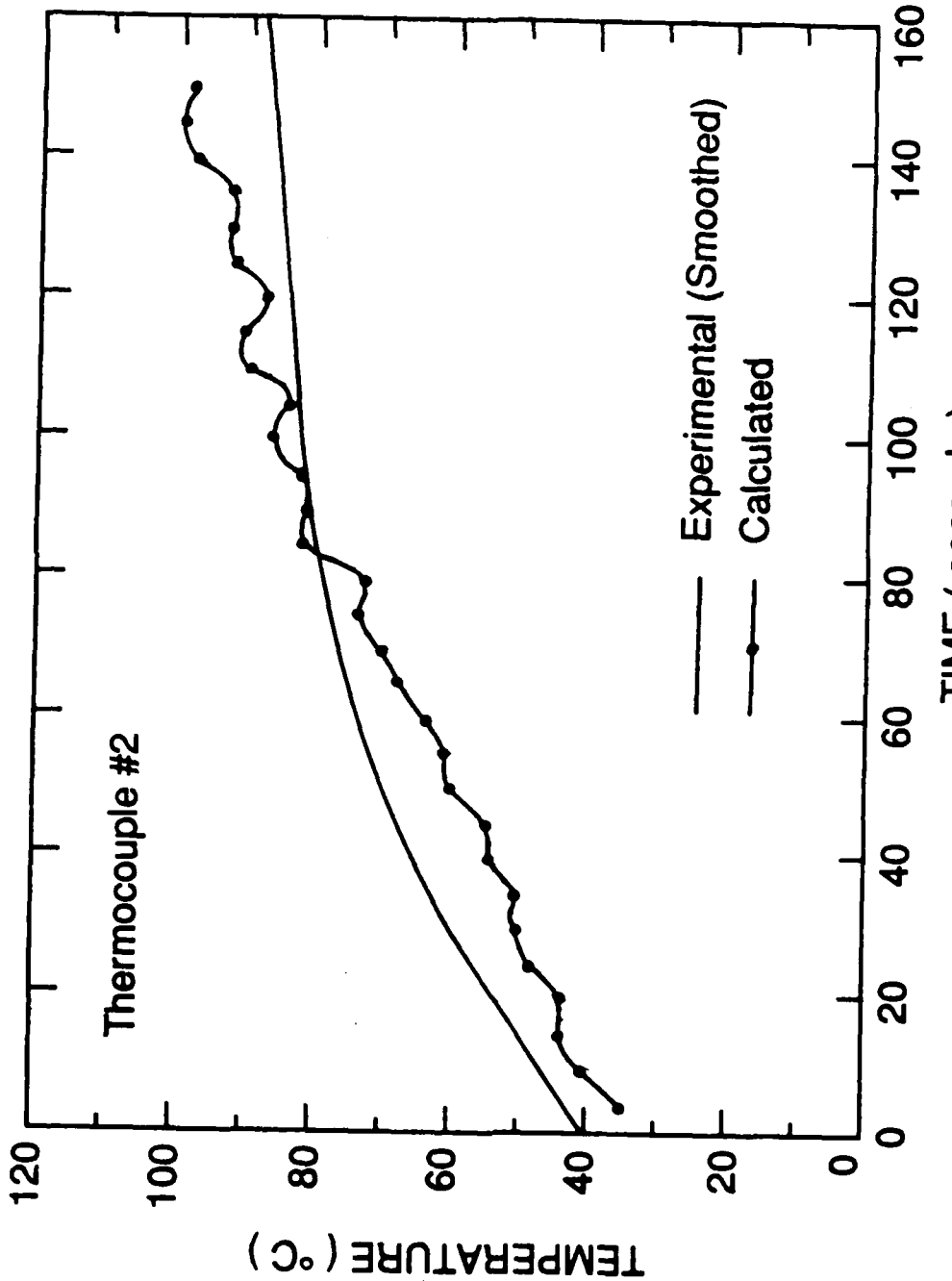

Figure 6. Temperature Comparison at Thermocouple #2 Location.

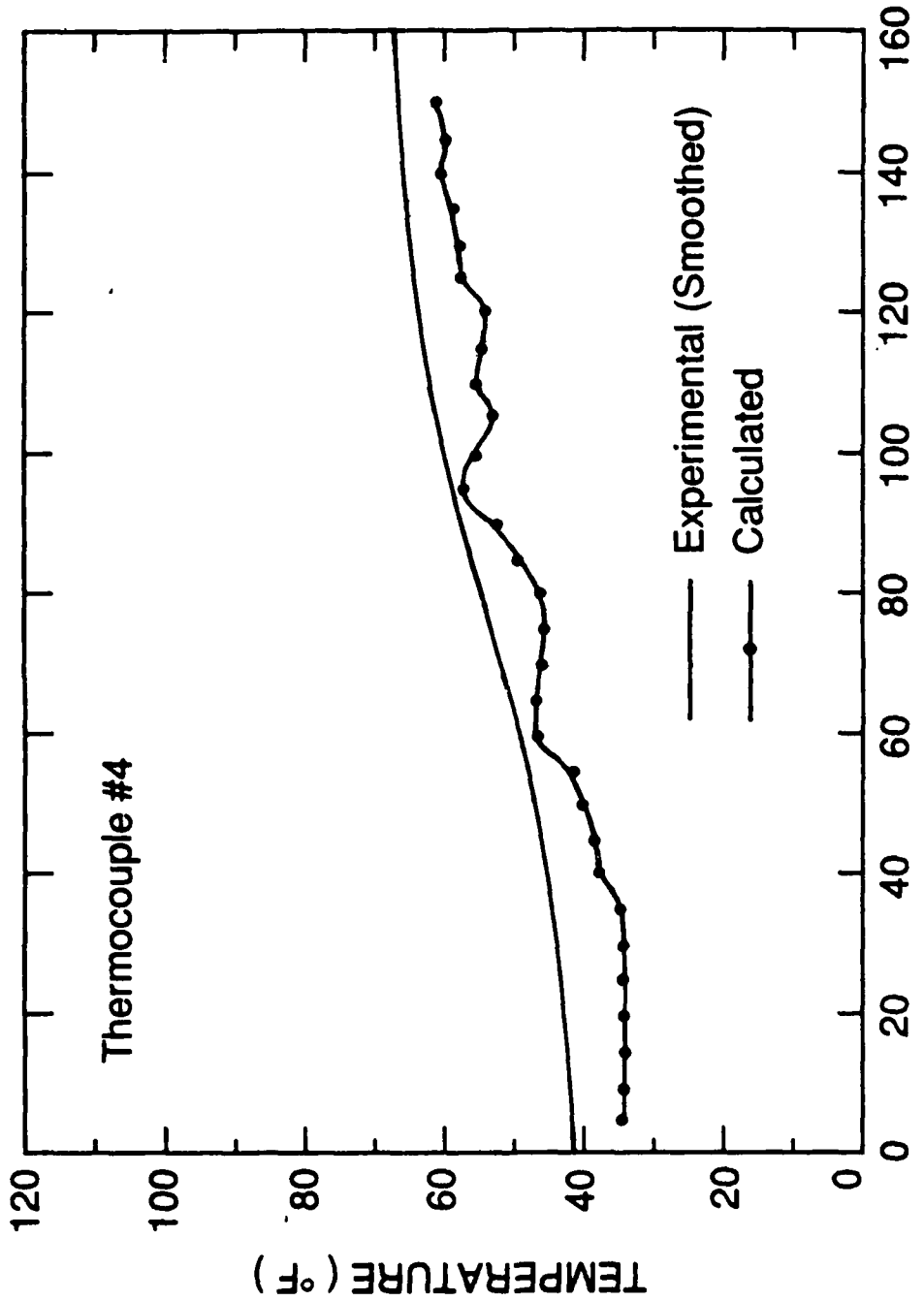

Figure 7. Temperature Comparison at Thermocouple #4 Location

possible reason is that gas and soot radiation is neglected in the field model. Since in general the effect of gas and soot radiation is to make the temperature field more uniform in the enclosure (Yang, 1986), the thermocouple 1 location would also tend to have lower temperatures. Also, the uncertainty in the experimental heat release rate itself could also be responsible for the degree of discrepancy shown in Fig. 5. Incidentally, it is noted in Figs. 5, 6 and 7 that all calculated temperatures exhibit slow oscillations which cannot be attributed to turbulence. Such oscillations could very well be real because of inherent thermal instability associated with thermal plumes (Yang et al., 1983).

One of the major advantages of the field model is the fact that the numerical solution gives detailed spatial and temperal variations of the velocity and temperature fields. Such information is critical in the development of fire mitigation measures, especially in the placement of barriers and partitions, and in the determination of fire loads on the walls. The field results from the calculations in terms of the velocities and temperaturess can now be shown. Because of the three-dimensional nature of the fields, it is necessary to look at these quantities at specific sections of the tank. At a time instant 30 seconds into the fire, the isotherms, or the temperature field, and the velocity vector field are shown in Figs. 8. Fig. 8(a) gives a front view of these fields at the mid section of the tank. Fig. 8(b) refers to the view also at the mid section from the south end of the tank, while Fig. 8(c) is another view from the south end, but at the intersection between the end cap and the cylindrical mid section, or at the base of the end cap. Some sections are used in Figs. 9, 10, 11 and 12 at 60 seconds, 90 seconds, 120 seconds and 150 seconds from the commencement of the fire, respectively.

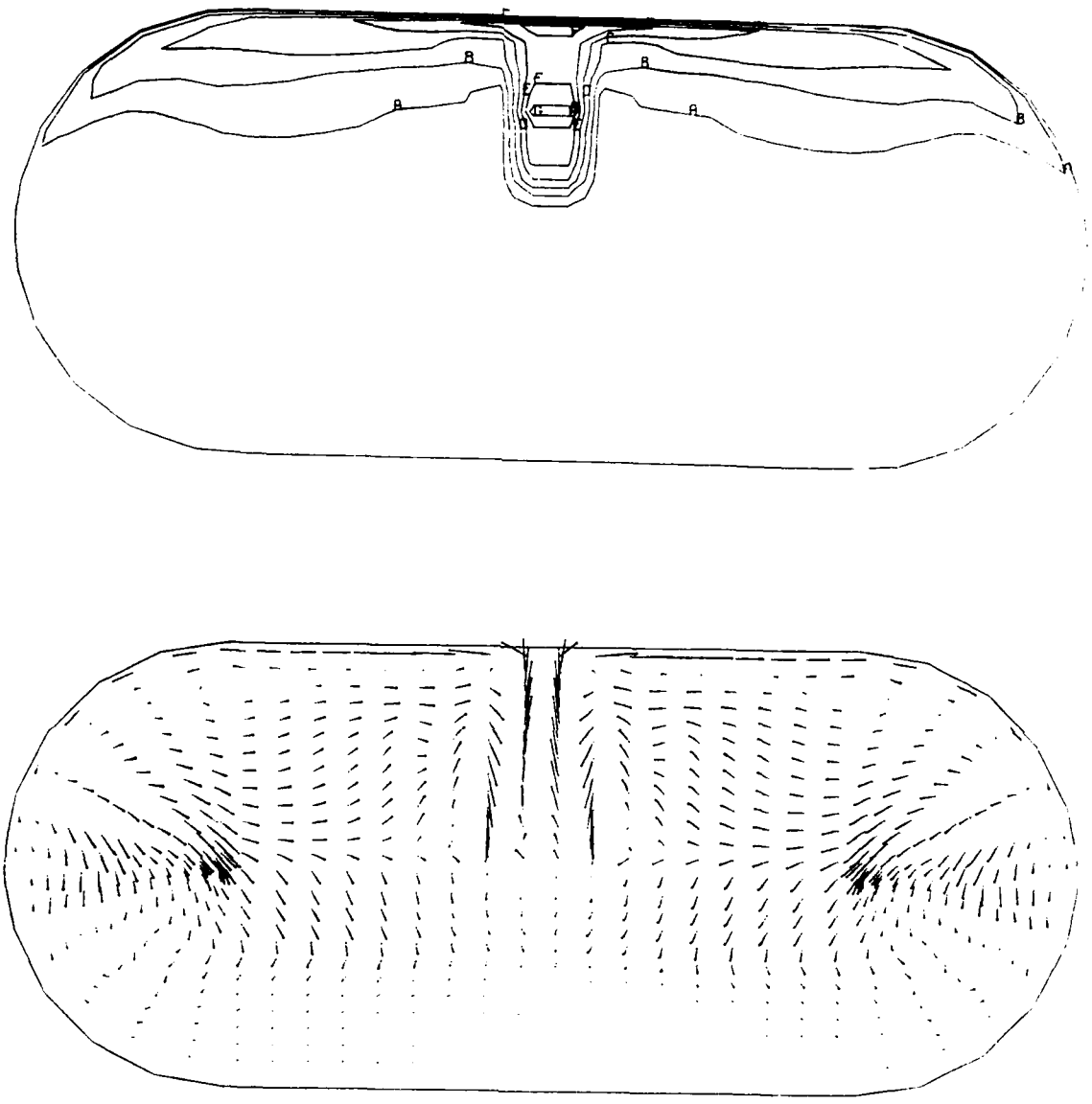

Figure 8(a). Mid-Section Front View of Isotherms and Velocity Field at 30 seconds

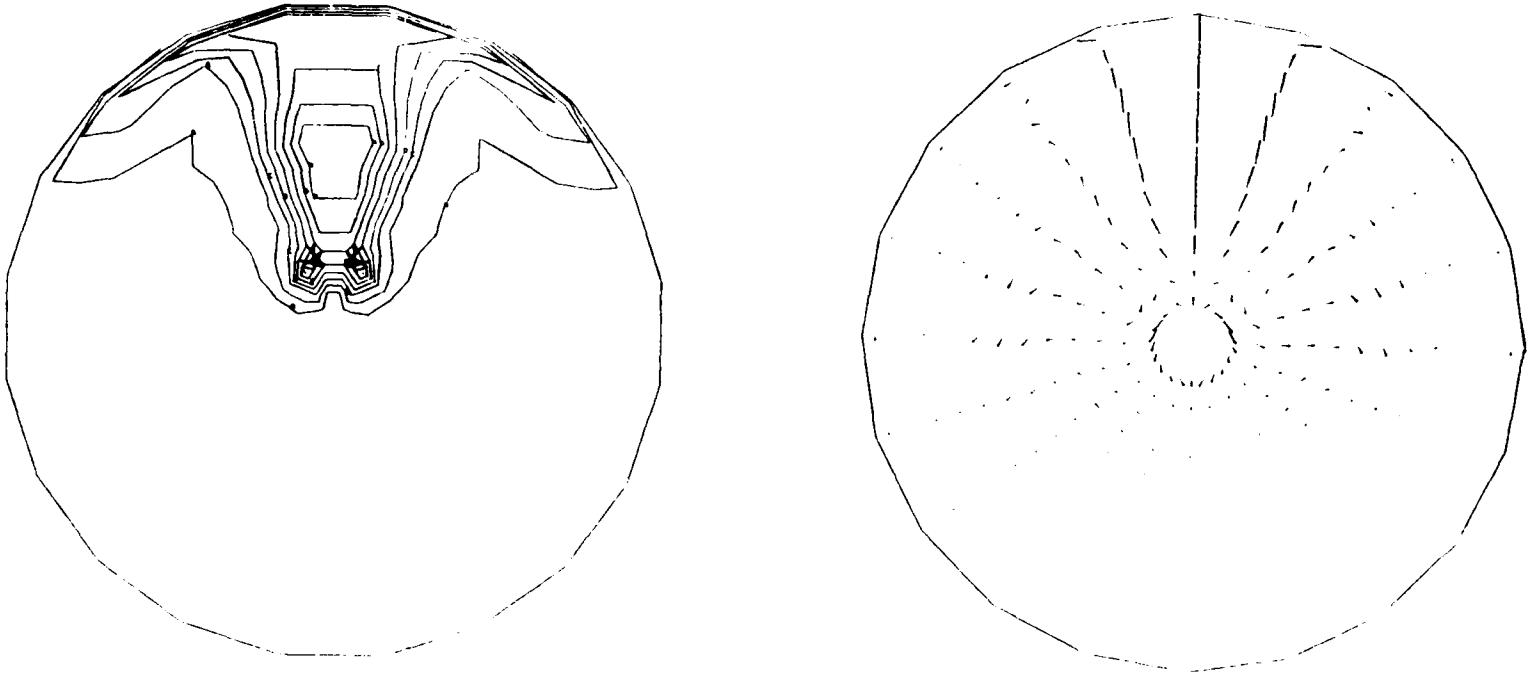

Figure 8(b). Mid-Section End View of Isotherms and Velocity Field at 30 seconds

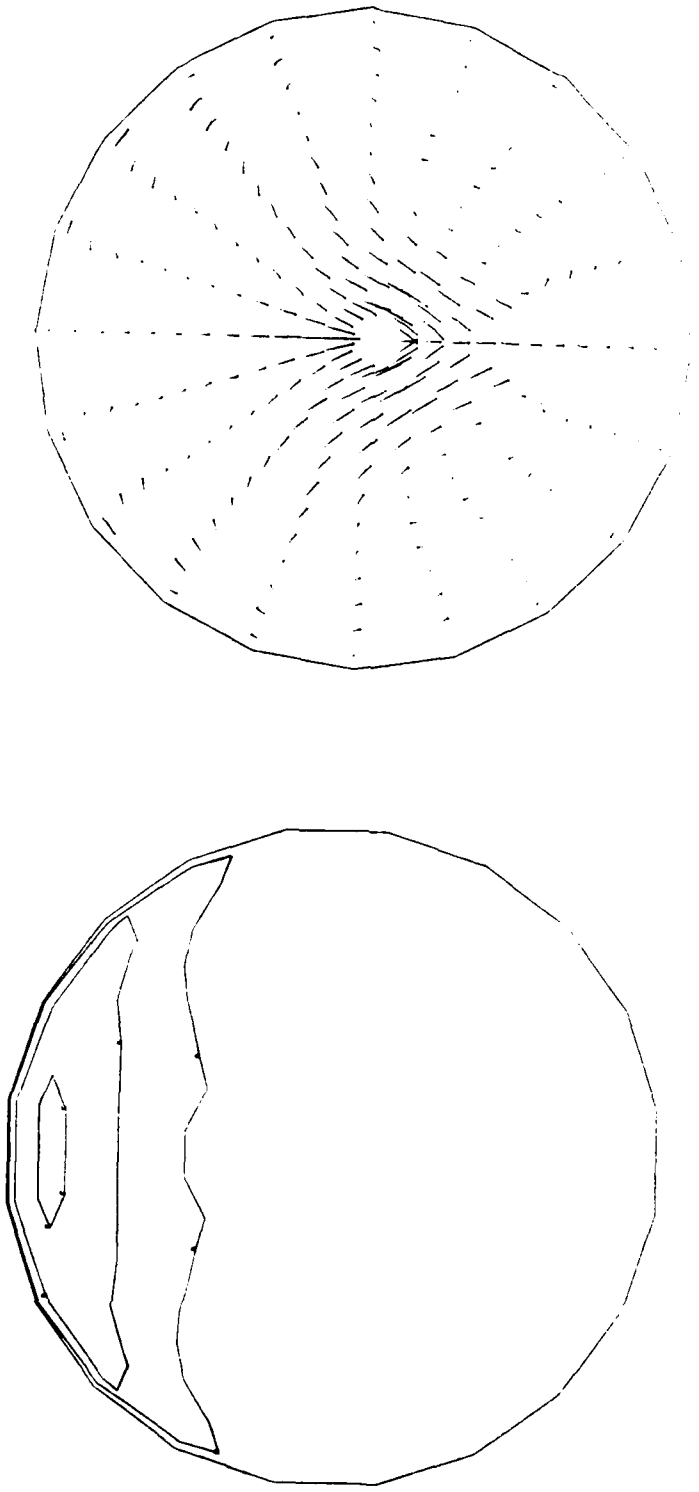

Figure 8(c). Section View at Base of End Cap of Isotherms and Velocity Field at 30 seconds

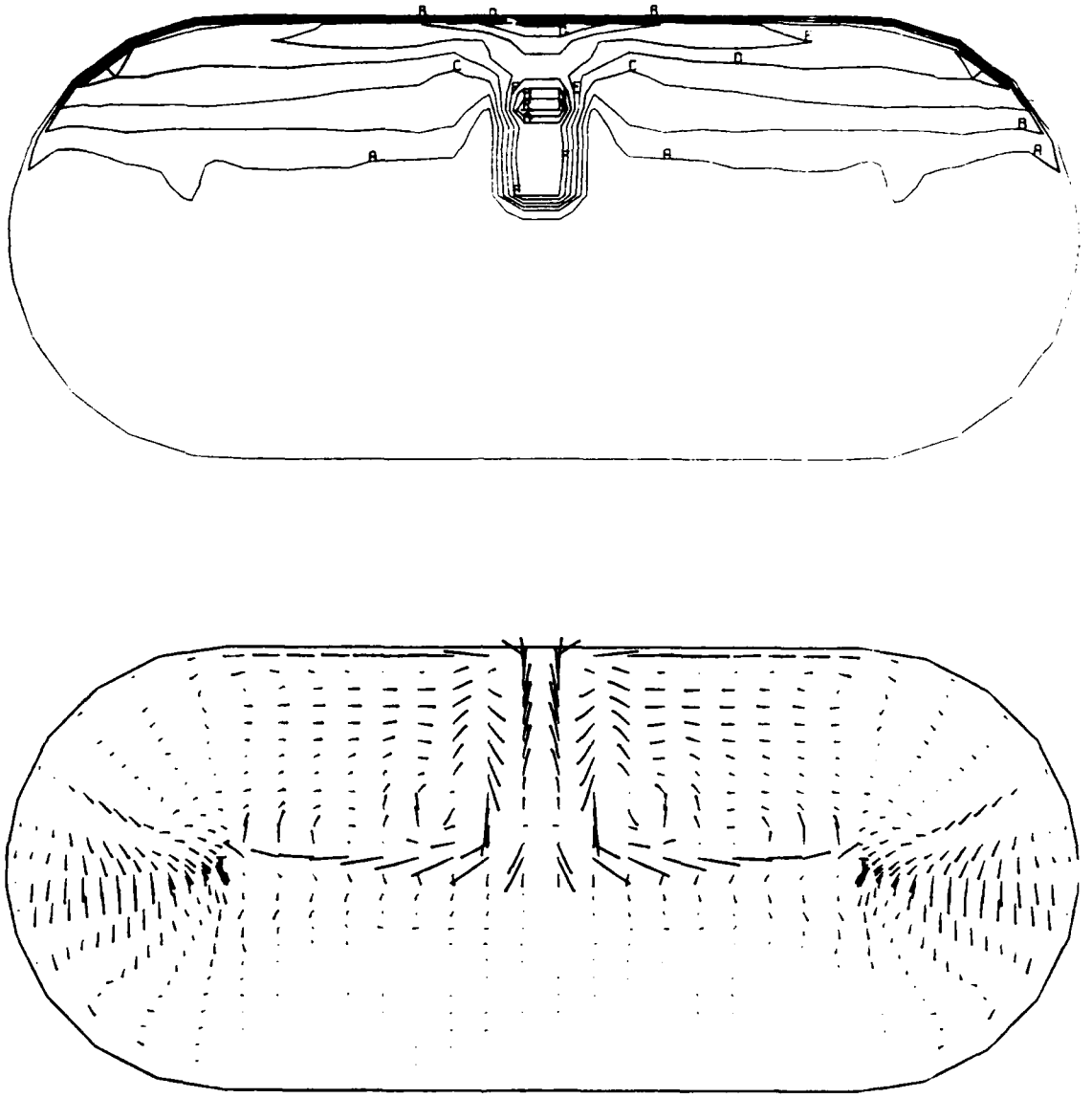

Figure 9(a). Mid-Section Front View of Isotherms and Velocity Field at 60 seconds.

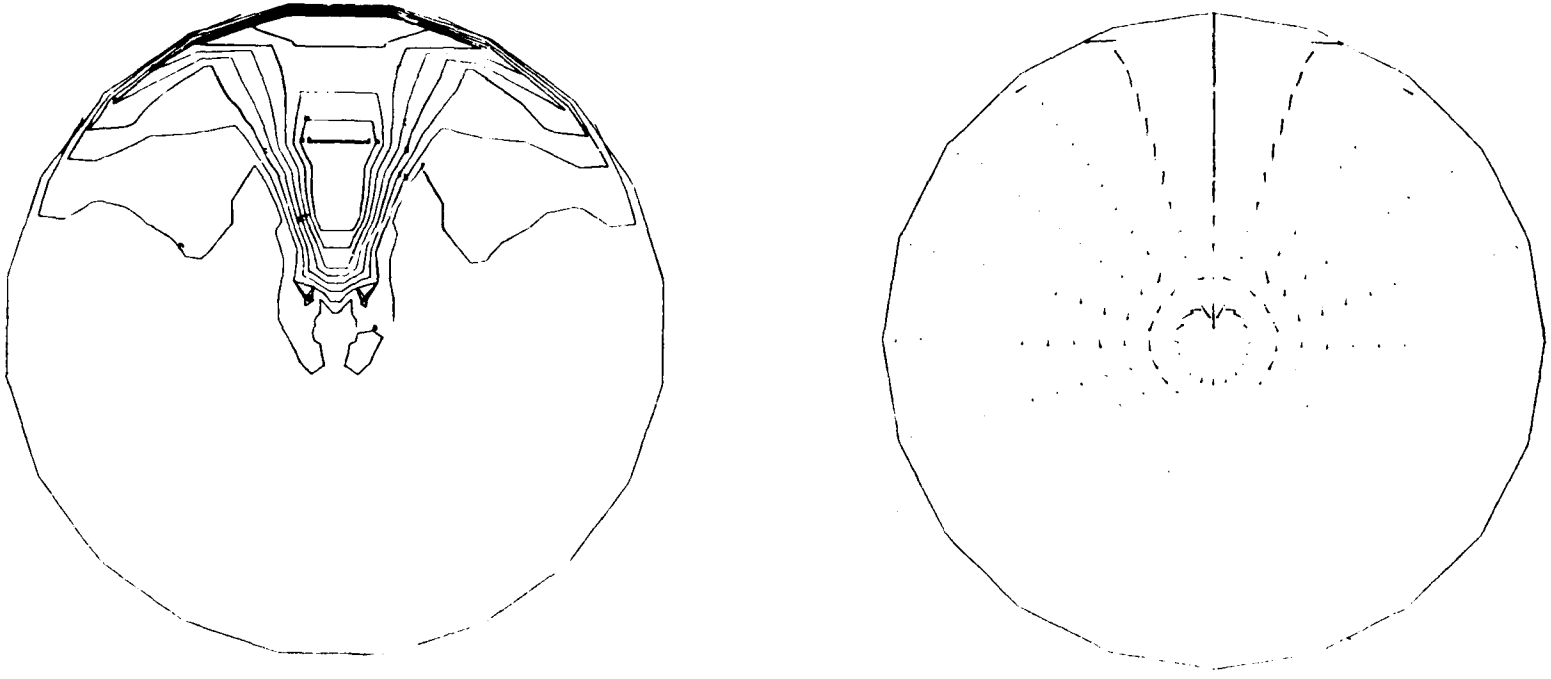

Figure 9(b). Mid-Section End View of Isotherms and Velocity Field at 60 seconds

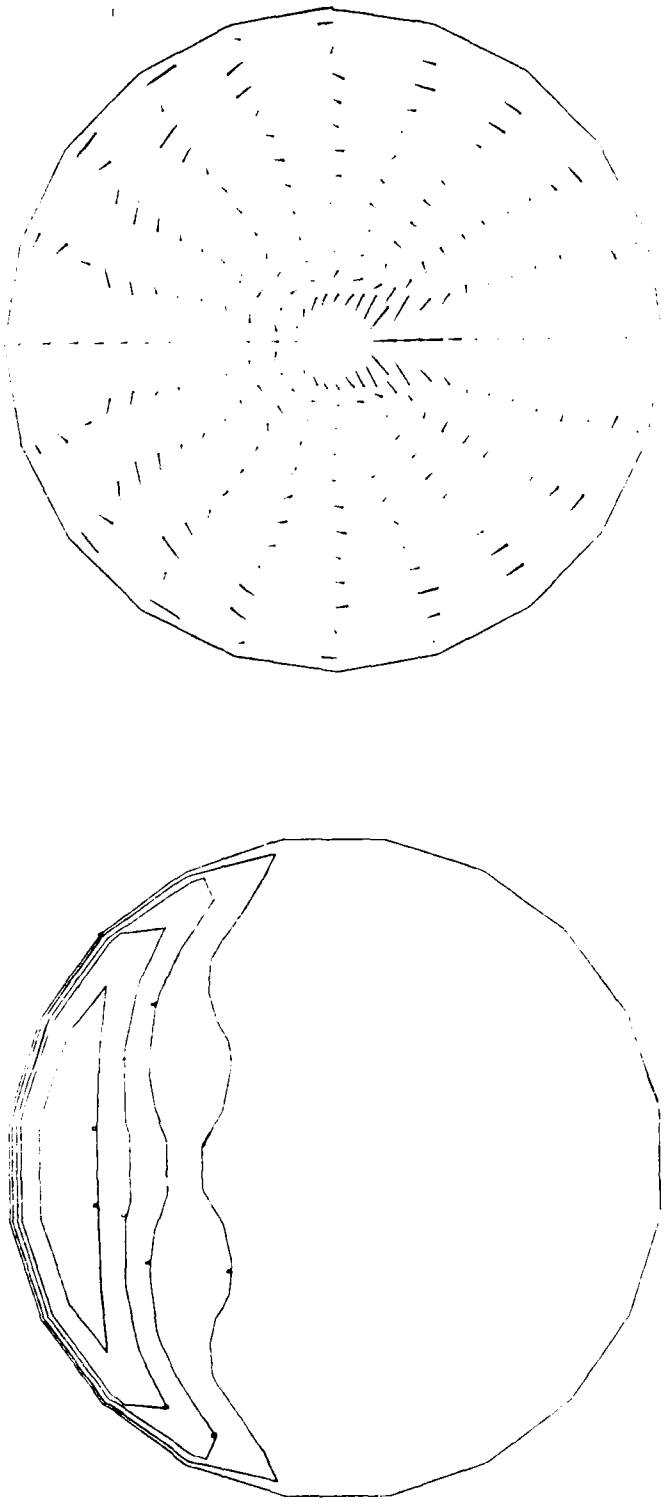

Figure 9(c). Section View at Base of End Cap of Isotherms and Velocity Field at 60 seconds

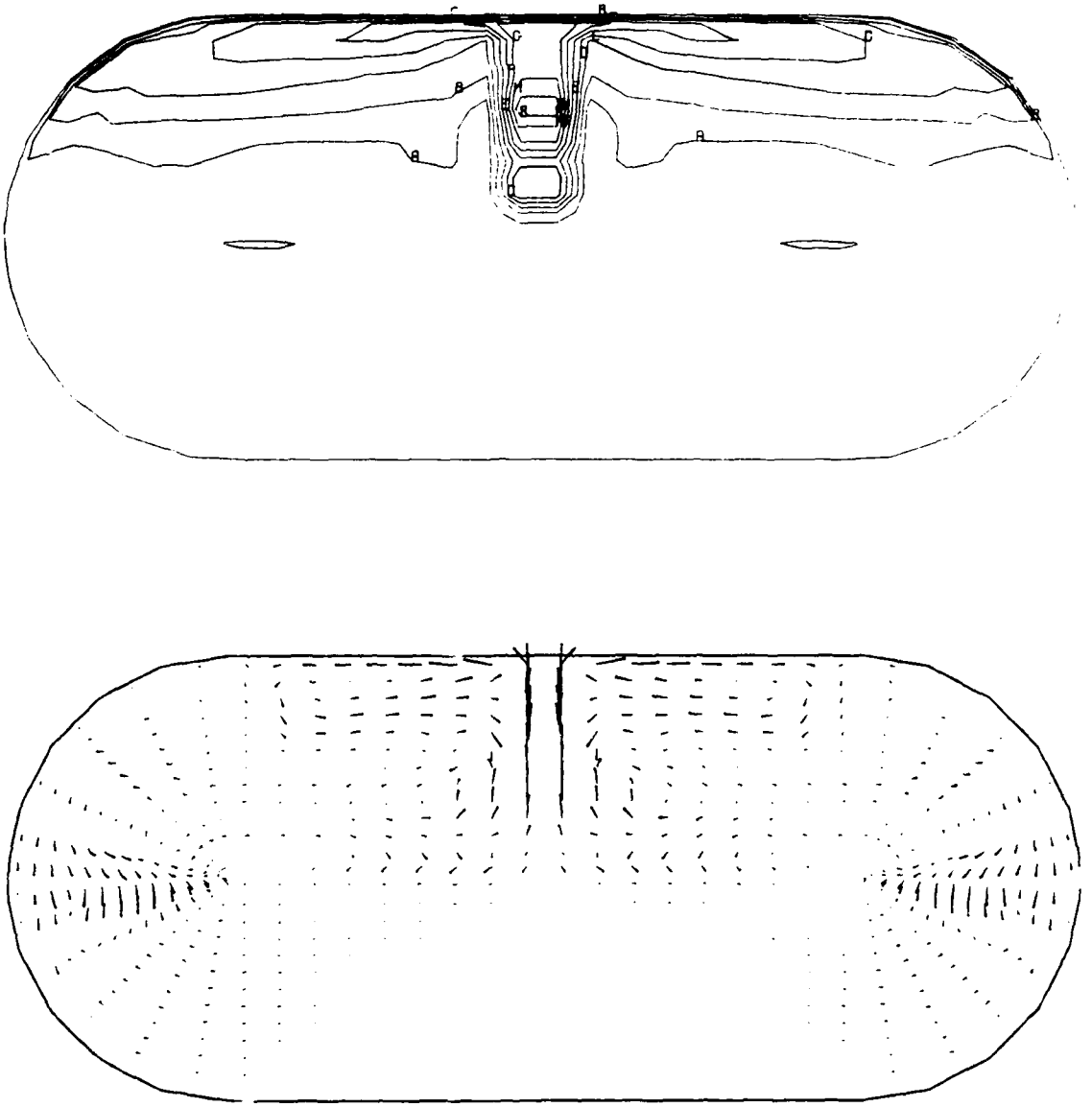

Figure 10(a). Mid-Section Front View of Isotherms and Velocity Field at 90 seconds

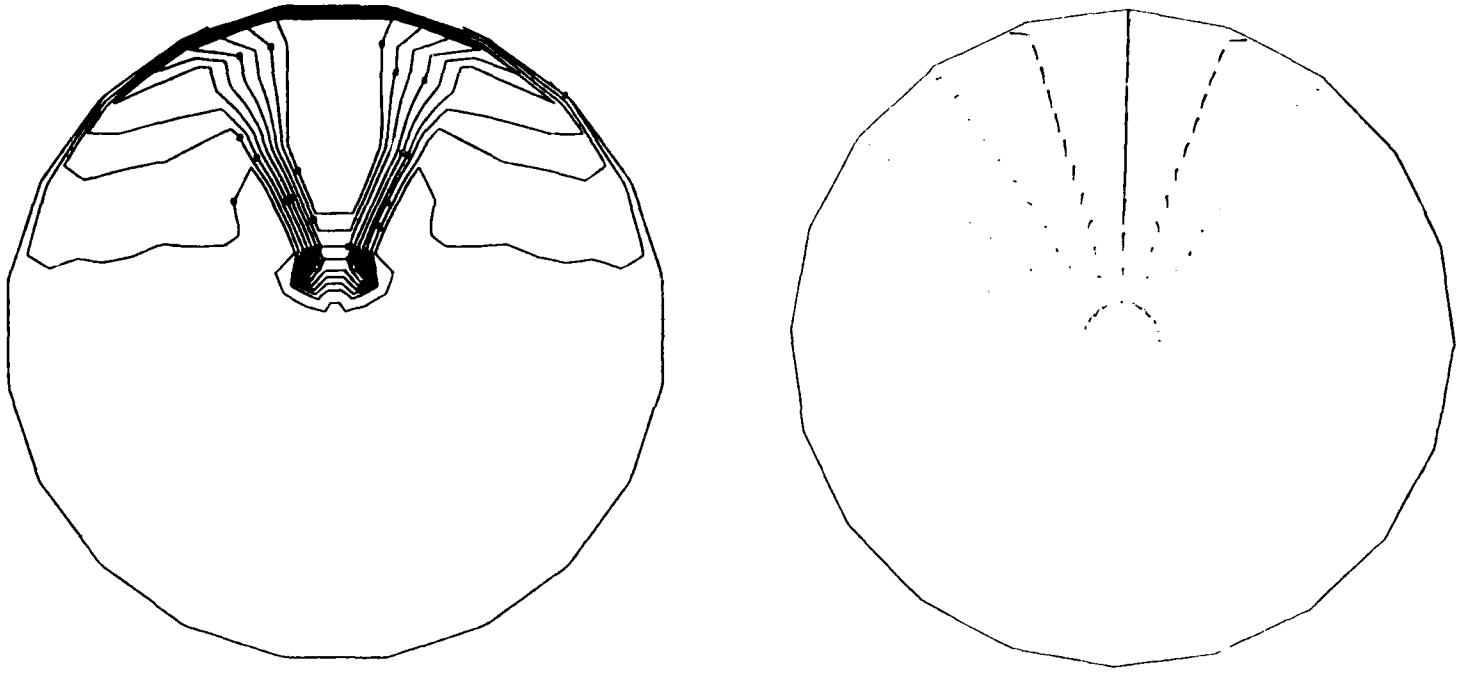

Figure 10(b). Mid-Section End View of Isotherms and Velocity Field at 90 seconds

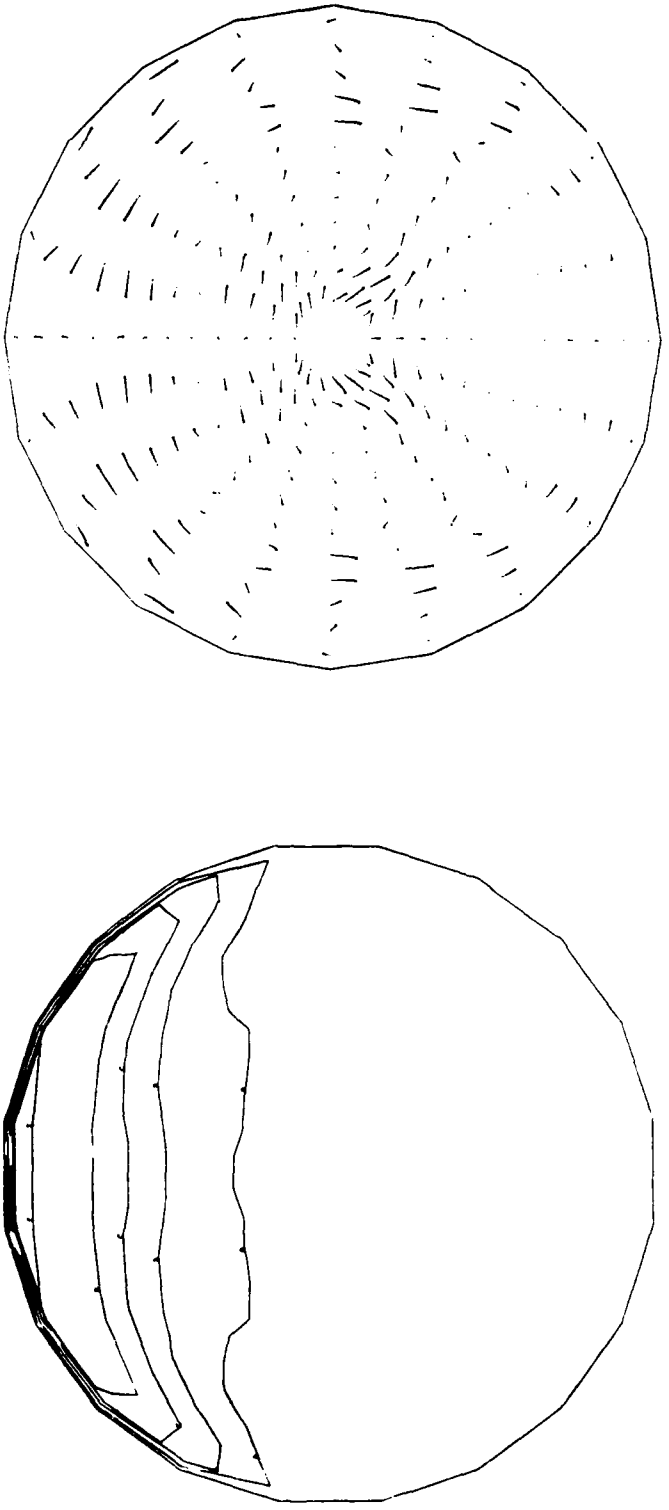

Figure 10(c). Section View at Base of End Cap of Isotherms and Velocity Field at 90 seconds

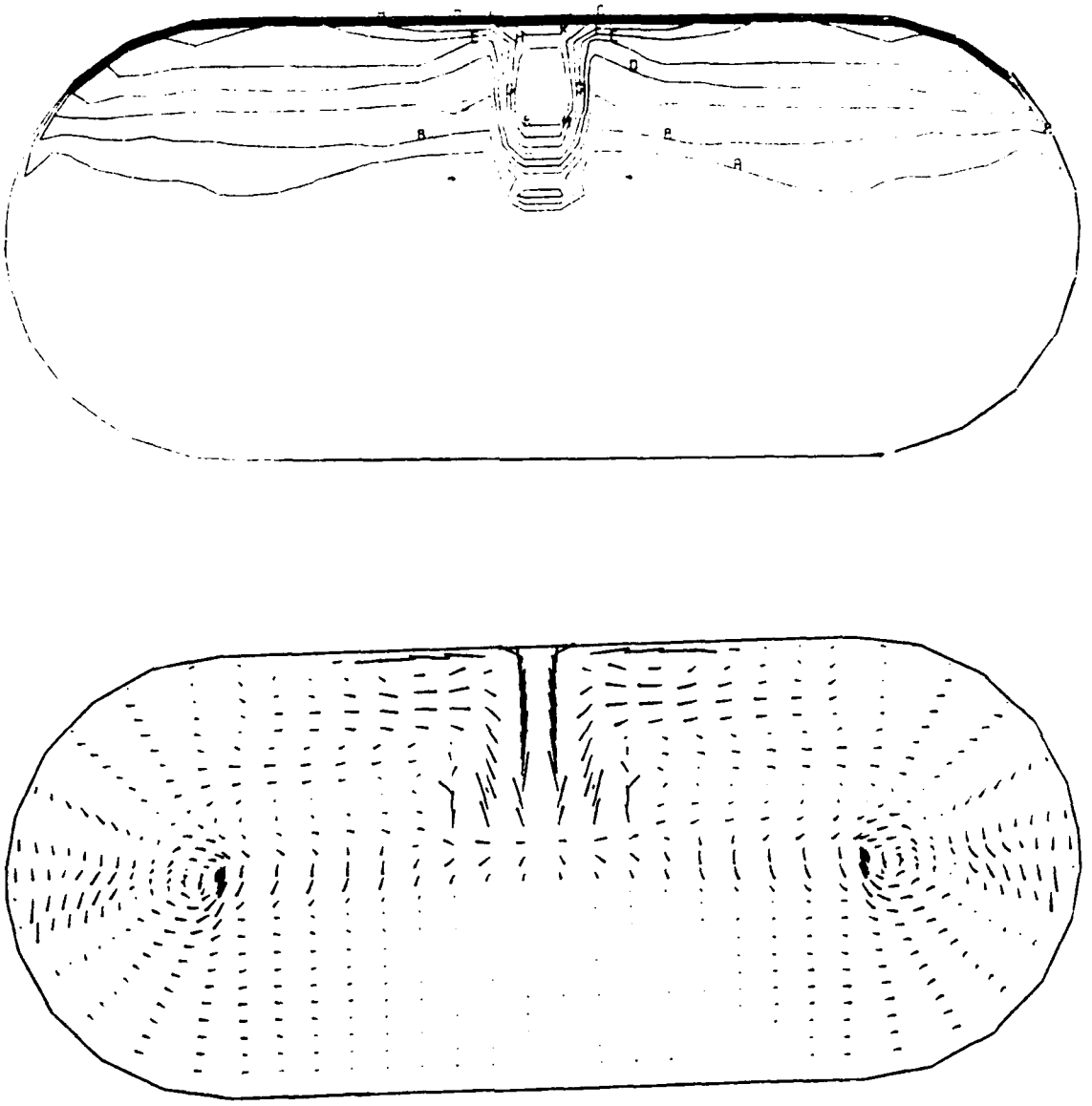

Figure 11(a). Mid-Section Front View of Isotherms and Velocity Field at 120 seconds.

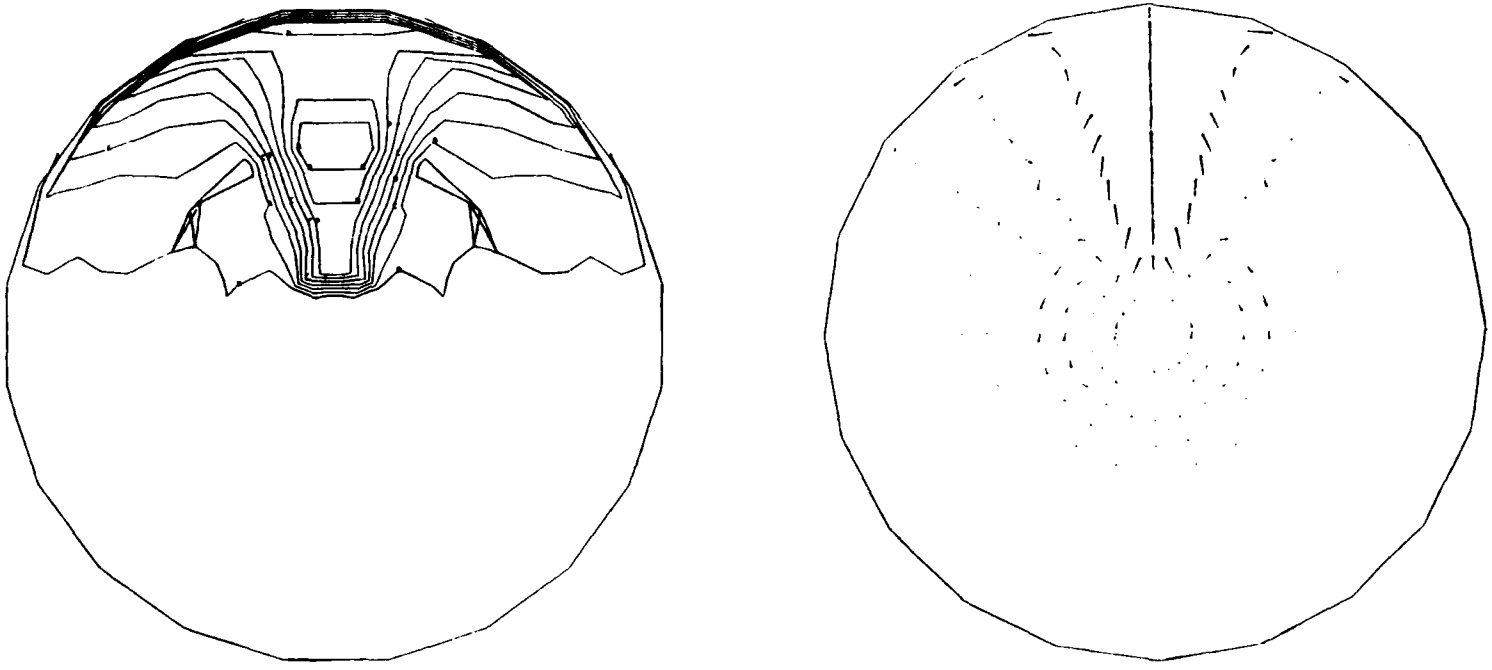

Figure 11(b). Mid-Section End View of Isotherms and Velocity Field at 120 seconds.

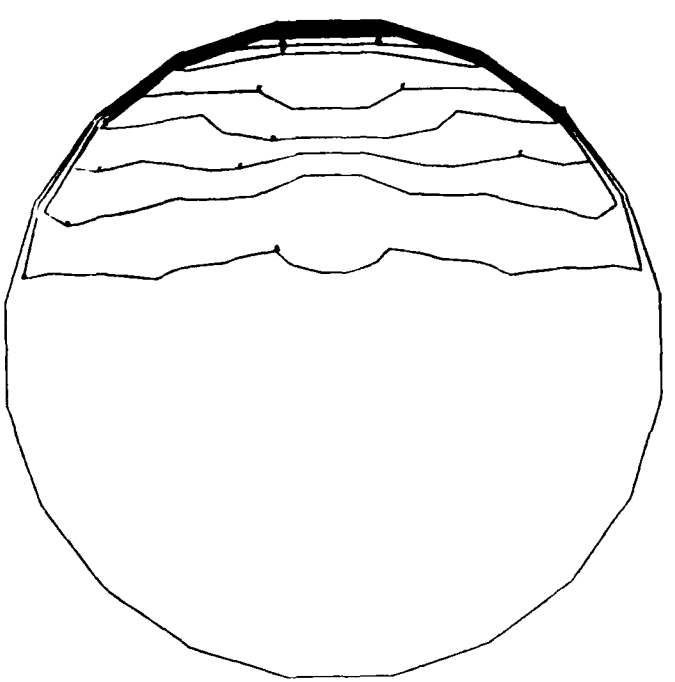

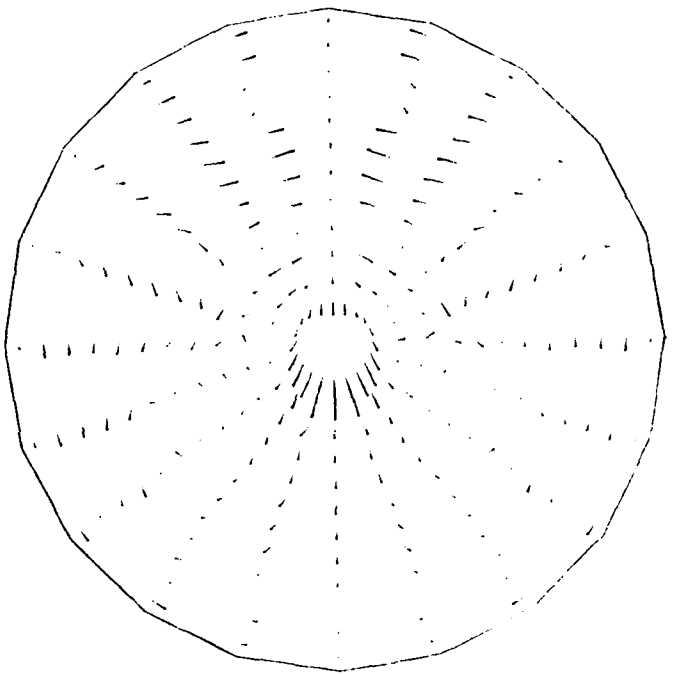

Figure 11(c), Section View at Base of End Cap of Isotherms and Velocity Field at 120 seconds

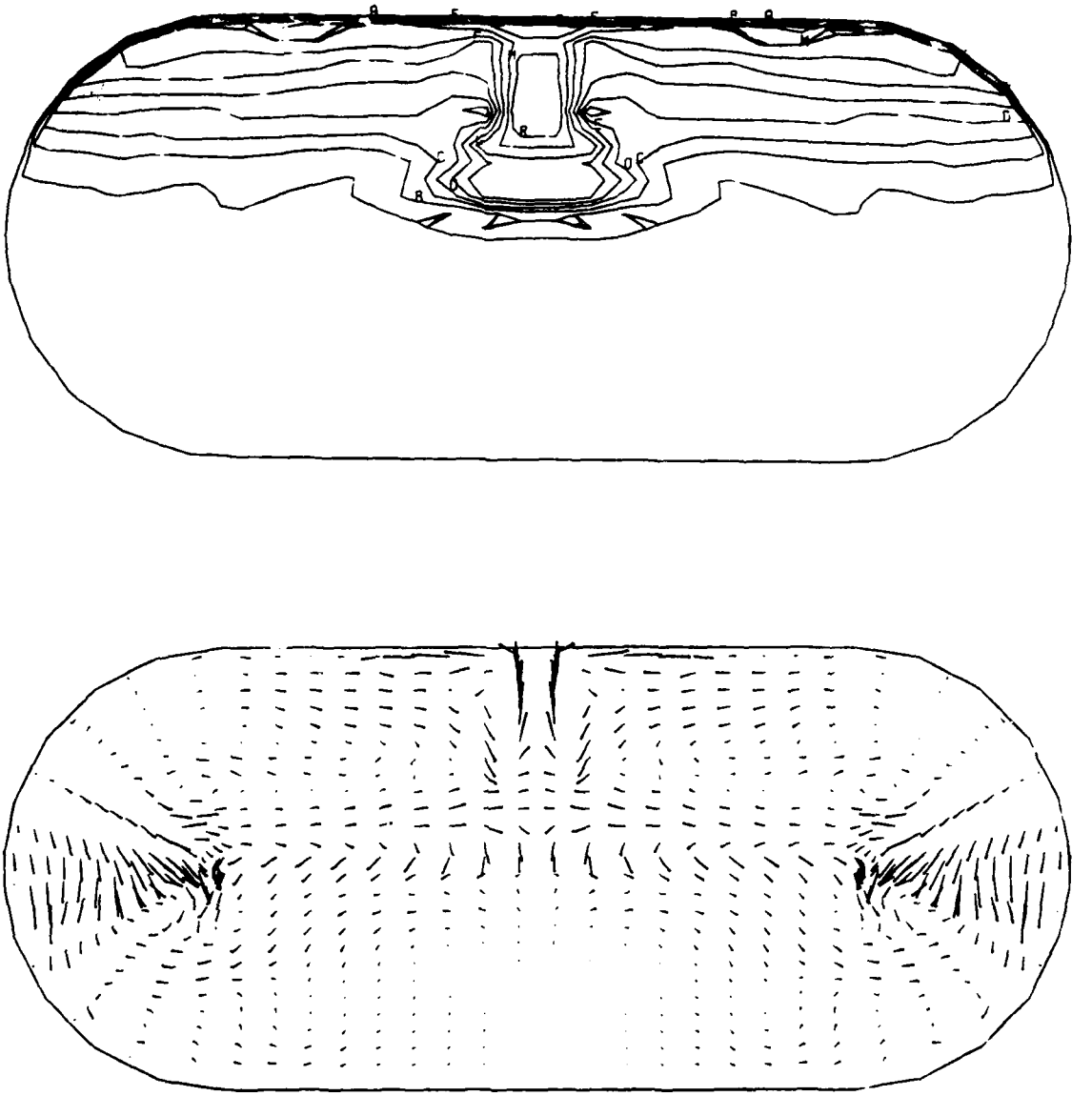

Figure 12(a). Mid-Section Front View of Isotherms and Velocity Field at 150 seconds

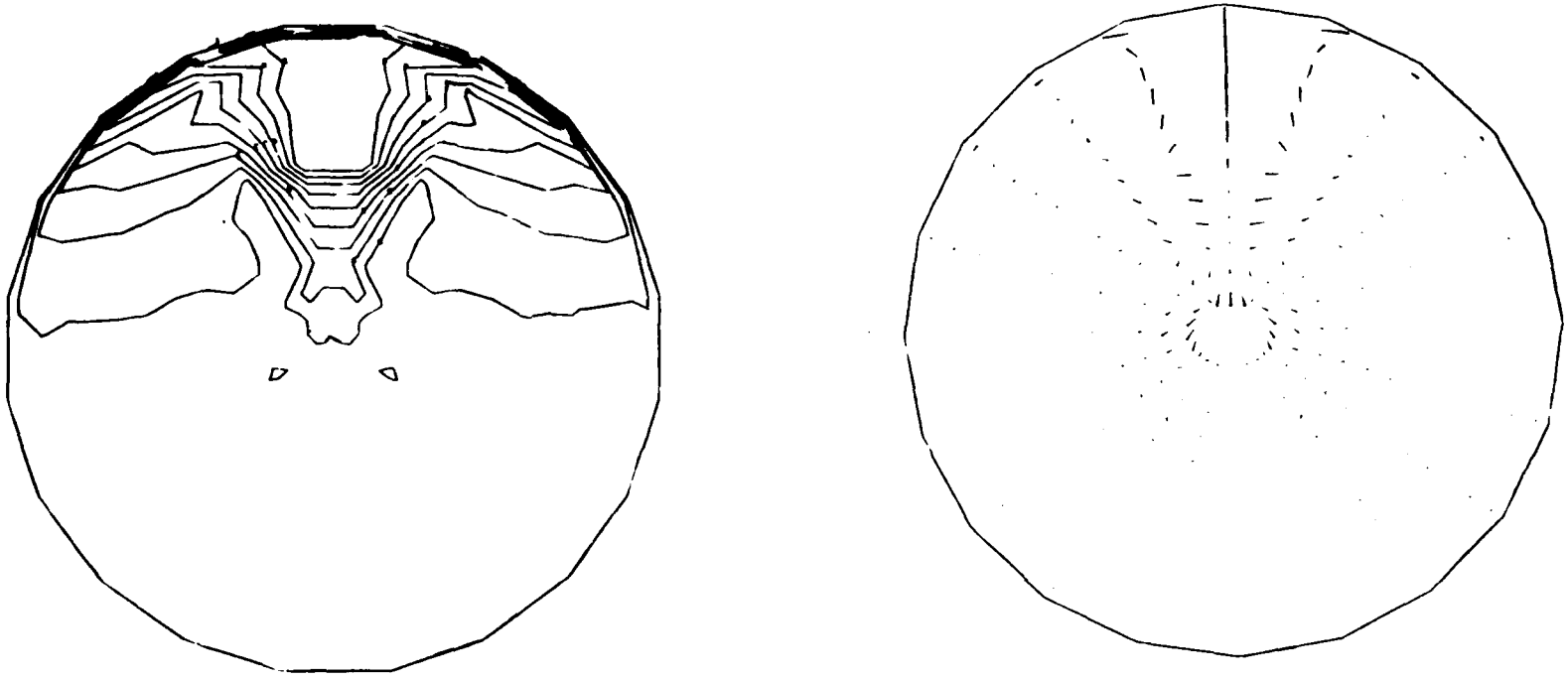

Figure 12(b). Mid-Section End View of Isotherms and Velocity Field at 150 seconds

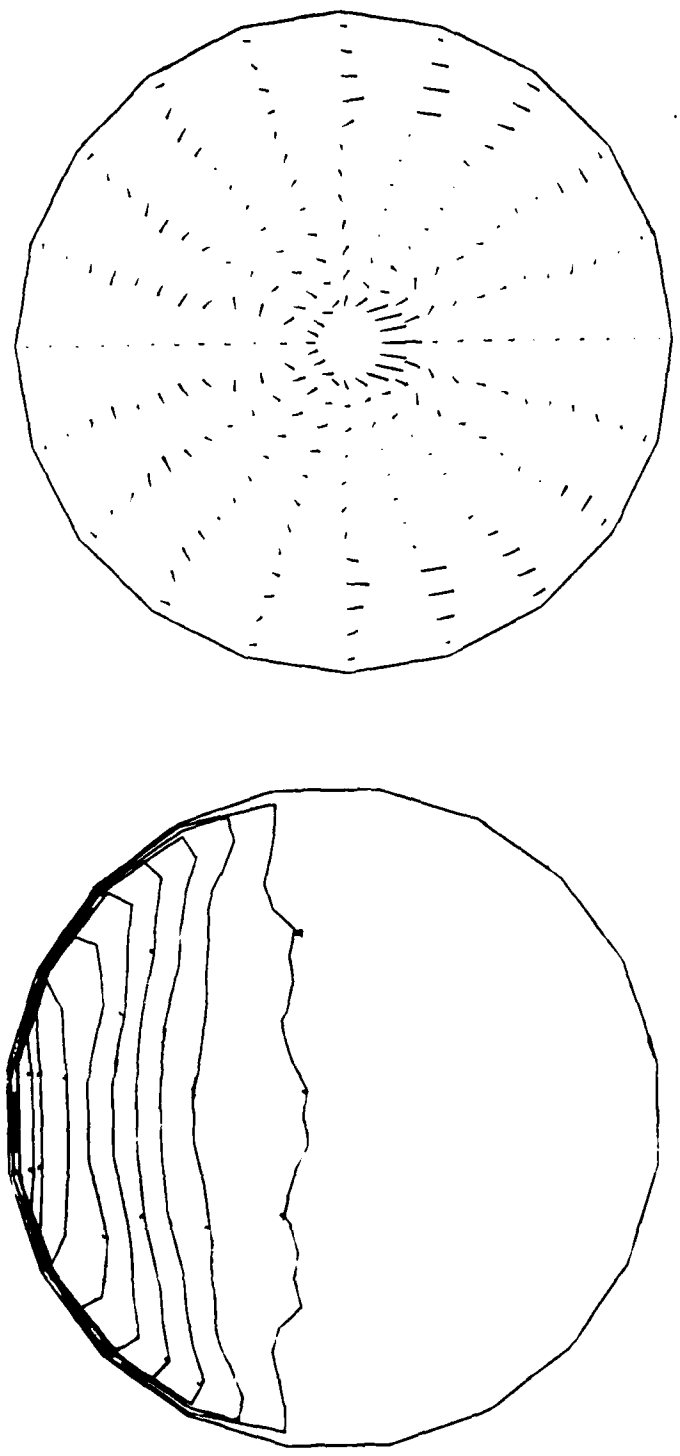

Figure 12(c). Section View at Base of End Cap of Isotherms and Velocity Field at 150 seconds.

Since the fire is located at the center of the tank, both sections in Figs. 8(a) and 8(b) include the flame, and therefore it is seen that the fire plume is already well formed at 30 seconds. There is also a hot ceiling layer along the ceiling of the tank, and the lower two thirds of the tank are still at almost the initial temperature. The general flow circulation pattern is much more complex than might be expected. The entrainment into the fire plume is limited to the immediate neighborhood of the fire, as can be seen in Figs. 8(a) and 8(b). The flow in the hot ceiling layer does not seem to have strong enough momentum to carry the flow toward the lower half of the tank, but returns into the tank interior, resulting in a downward-biased flow even at the section as shown in Fig. 8(c). The flow completes its journey back toward the fire region in a somewhat spatially oscillatory path. At 60 seconds as shown in Fig. 9, the depth of the hot ceiling layer is increased, even though the lower half of the tank is still not affected much by the fire. The flow in the ceiling layer toward and down the spherical end cap is definitely spiral in nature. In addition, the spatially oscillatory flow back to the fire zone become sufficiently large that it induces a backward flow toward the end cap again at the bottom of the fire. It may also be of interest to note that the isotherms are now more densely packed at the ceiling region of the tank, indicating that heat losses through the wall now become more important. Similar trends of the temperature and velocity fields can be seen at 90, 120 and 150 second instants in Figs. 10, 11 and 12, respectively. It is interesting to note that the hot ceiling layer reaches down almost to the half tank height level at 120 and 150 seconds, and inside the hot layer, the temperature field is essentially stably stratified except a small thermal bounday layer region

next to the ceiling. Incidentally, the isotherm and velocity vector scales in Figs. 8 to 12 are not uniform, and consequently the diagrams should not be used quantitatively for comparison purposes.

CONCLUDING REMARKS

The present study develops a three-dimensional differential field model based on general orthogonal coordinate systems which includes the physical effects of turbulence, strong buoyancy, full compressibility, surface-surface and surface-flame radiation exchange, pressure rise due to fire loading, and heat losses through the wall. The model is capable of dealing with geoometries that represent enclosures with combinations of shapes which are describable by orthogonal coordinates. The model, which is also based on a control-volume finite-difference approach with primitive variables, staggered cells, and QUICK scheme, and both local and global pressure corrections, is used to simulate a set of full-scale fire test data obtained in the NRL FIRE I fire test facility, which is a pressure vessel with a cylindrical mid-section and hemispherical end caps on both ends. Despite some uncertainty in the heat release-rate input data, reasonable comparisons in both the temperature levels at selected points in the test tank and the tank pressure between the calculated and test results have been obtained. However, there is also indication that the calculated temperatures close to the tank ceiling overpredict the test values, and possible reasons for this discrepancy have been noted.

Since the completion of this study, two additional capabilities of the field model have been developed and these include effects of recirculating fans to provide ventilation inside the test tank and the placement of

horizontal deck inside the tank. At the present time, the field model treats the fire as a volumetric heat source with prescribed heat release rate. Efforts have been initiated to develop a combustion model so that the fire envelope and heat release rate do not need to be prescribed. Furthermore, plans are also being made to incorporate a gas and soot (smoke) radiation model and a more refined turbulence model into the overall field model. Results of these efforts will be reported at future dates.

ACKNOWLEDGMENT

This study is sponsored by the Department of Navy under number N62271-87-M-0170 with the Naval Postgraduate School, which in turn has a sub-contract with the University of Notre Dame. The authors are particularly grateful to Dr. Pat Tatem of NRL for her guidance and help.

NOMENCLATURE

A	boundary areas of control volumes, m^2
A_i	radiating surface, m^2
B_i	radiosity, w/m^2
c_p	isobaric heat capacity, kJ/kgK
c_{pm}	mean isobaric heat capacity, Eq. (4), kJ/kgK
F_{ij}	radiation view factor
G_i	components of gravity vector, m/s^2
G_{ij}	radiation matrix, Eq. (41)
g	determinant of g_{ij}
g_{ij}	covariant metric tensor
g^{ij}	contravariant metric tensor
$\vec{g}$	gravity vector
$\vec{g}_i$	base vector
H	enclosure height, m
h	coefficient of heat transfer, w/m^2K
h_i	scale factor
J^i	total heat flux, w/m^2
K	constant in turbulence model
k	thermal conductivity, W/mK
L_w	thickness of wall, m
ℓ	mixing length, Eq. (21), m
M^{ij}	total momentum flux, N/m^2
$\hat{M}^{ij}$	momentum flux, Eq. (29), N/m^2
$\hat{n}$	outward normal
Pr	Prandtl number

Pr_t	turbulent Prandtl number
p	static pressure, N/m^2
Q	heat source w/m^3
q_c	conduction flux, w/m^2
q_r	radiation flux, w/m^2
R	gas constant, Nm/kgK
R_i	gradient Richardson number, Eq. (20)
R_{ij}	line between surfaces i and j
r	radius variable, m
S	source term, N
$\hat{S}$	source term, Eq. (31),N
T	absolute temperature, K
T_o	outside ambient temperature, K
u_i	velocity components in X_i system, m/s
u^i	velocity components in θ^i system, m/s
X_{ij}	matrix components, Eq. (37)
X_{ij}^{-1}	inverse of X_{ij}
x_i	Cartesian coordinates, m
β_i	angle between normal to A_i and R_{ij}, rad
ΔV	control volume, m^3
δ_{ij}	Kronecke delta
ϵ_i	surface emissivity
θ	circumferential angle, rad
θ^i	orthogonal coordinate
μ	viscosity, kg/ms
ρ	density, kg/m^3

σ Stefan-Boltzmann constant, w/m^2K^4

σ_{ij} shear stress tensor, N/m^2

σ^j_{ij} shear stress tensor in θ^i system, N/m^3

$\hat{\sigma}^j_i$ shear stress tensor, Eq. (28), N/m^2

ϕ polar angle, rad

Subscripts

eff effective (laminar + turbulent)

R reference quantities

s solid

t time derivative

REFERENCES

Alexander, J.I., St. Aubin, H.J., Stone, J.P., Street, T.T., and Williams, F.W., 1982. Large-Scale Pressurizable Fire Test Facility-FIRE I, NRL Report 8643, Naval Research Laboratory, Washington, D.C.

Bagnaro, M., Laouisset, M., and Lockwood, F.C., 1983. Field Model Prediction of Some Room Fires: Steady and Transient, in Fire Dynamics and Heat Transfer, ASME HTD-Vol. 25, New York, pp. 107-114.

Baum, H.R., and Rehm, R.G., 1984. Calculations of Three-Dimensional Buoyant Plumes in Enclosures, Combustion Science and Technology, Vol. 40, p. 55-77.

Chang, L.C., Yang, K.T., and Lloyd, J.R., 1983. Radiation-Convection Interaction in Two-Dimensional Complex Enclosures, Journal of Heat Transfer, Vol. 105, pp. 89-95.

Kou, H.S., Yang, K.T., and Lloyd, J.R., 1986. Turbulent Buoyant Flow and Pressure Variations Around an Aircraft Fuselage in a Cross Wind Near the Ground, Proceedings of the First International Symposium on Fire Safety Science, Hemisphere Publishing Corp., Washington,D.C., pp. 173-184.

Leonard, B.P., 1983. A Convective Stable, Third-Order Accurate Finite Difference Method for Steady Two-Dimensional Flow and Heat Transfer, in Numerical Properties and Methodologies in Heat Transfer, ed. T.M. Shih, Hemisphere Publishing Corp., Washington, D.C., pp. 211-226.

Lloyd, J.R., Yang, K.T., and Liu, K.V., 1979. A Numerical Study of One-Diomensional Surface, Gas and Soot Radiation for Turbulent Buoyant Flows in Enclosures. Proceedings of the 1st National Conference on Numerical Methods in Heat Transfer, College Park, MD., pp. 142-161.

Markatos, N.C., Malin, M.R., and Cox, G., 1982. Mathematical Modeling of Buoyancy Induced Smoke Flow in Enclosures, International Journal of Heat and Mass Transfer, Vol. 25, pp. 63-75.

Markatos, N.C., and Pericleous, K.A., 1983. An Investigation of Three-Dimensional Fires in Enclosures, in Fire Dynamics and Heat Transfer, ASME HTD-Vol. 25, New York, pp. 115-124.

Nicolette, V.F., Yang, K.T., and Lloyd, J.R., 1985. Transient Cooling by Natural Convection in a Two-Dimensional Square Enclosure, International Journal of Heat and Mass Transfer, Vol. 28, pp. 1721-1732.

Nies, G.F., 1986. Numerical Field Model Simulation of Full-Scale Fire Tests in a Closed Vessel, Master's and Mechanical Engineeer's Thesis, Naval Postgraduate School, Monterey, CA.

Nee, V.W., and Liu, K.V., 1978. An Algebraic Turbulence Model for Buoyant Recirculating Flow, Technical Report TR-79002-78-2, Department of Aerospace and Mechanical Engineering, University of Notre Dame, Notre Dame, IN.

Raithby, G.D., Galpin, P.F., and Doormaal, J.P., 1986. Prediction of Heat and Fluid Flow in Complex Geometries Using General Orthogonal Coordinates, Numerical Heat Transfer, Vol. 9, pp. 125-142.

Raycraft, J.K., 1987. Numerical Field Model Simulation of Full Scale Fire Tests in a Closed Spherical/Cylindrical Vessel. M.S. and Mechanical Engineer's Thesis, Naval Postgraduate School, Monterey, CA.

Rockett, J.A., Morita, M., and Cooper, L.Y., 1987. Comparison of NBS/Harvard VI Simulations and Full-Scale, Multi-Room Fire Test Data, Report NBSIR 87-3567, National Bureau of Standards, Washington, D.C., 59 pp.

Satoh, K., Lloyd, J.R., Yang, K.T., and Kanury, A.M., 1983. A Numerical Finite Difference Study of the Oscillatory Behavior of Vertically Vented Compartments, in Numerical Properties and Methodologies in Heat Transfer, Ed. T.M. Shih, Hemisphere Publishing Corp., Washington, D.C., pp. 517-528.

Siegel, R., and Howell, J.R., 1981. Thermal Radiation Heat Transfer, 2nd Edition, Hemisphere Publishing Corporation, Washington, D.C.

Sparrow, E.M., and Cess, R., 1978. Radiation Heat Transfer, Hemisphere Publishing Corp., Washington, D.C.

Stroup, D.W., 1987. A Catalog of Compartment Fire Model Algorithms and Associated Computer Subroutines, Report NBSIR87-3607, National Bureau of Standards, Washington, D.C.

Yang, K.T., 1986. Numerical Modeling of Natural Convection-Radiation Interactions in Enclosures, Proceedings of the 8th International Heat Transfer Conference, Hemisphere Publishing Corp., Washington, D.C., Vol. 1, pp. 131-140.

Yang, K.T., and K.V. Liu, 1978. UNDSAFE-II. A Computer Code for Buoyant Turbulent Flow in an Enclosure with Thermal Radiation, Technical Report TR-79002-78-3, Department of Aerospace and Mechanical Engineering, University of Notre Dame.

Yang, K.T., and Lloyd, J.R., 1985. Turbulent Buoyant Flow in Vented Simple and Complex Enclosures, in Natural Convection: Fundamentals and Applications, eds. W. Aung, S. Kakac and R. Viskanta, Hemisphere Publishing Corp., Washington, D.C., pp. 303-329.

Yang, K.T., Lloyd, J.R., Kanury, A.M., and Satoh, K., 1984. Modeling of Turbulent Buoyant Flows in Aircraft Cabins, Combustion Science and Technology, Vol. 39, pp. 107-118.

Yang, H.Q., Yang, K.T., and Lloyd, J.R., 1987a. Three-Dimensional Finite Difference Calculations of Buoyant Flow in Arbitrary Parallelepiped Enclosures Using Curvilinear Non-Orthogonal Coordinates, Proceedings of the 5th International Conference on Numerical Methods for Thermal Problems, Vol. V, Pineridge Press, Swansea, UK, Part 2, pp. 1169-1181.

Yang, H.Q., Yang, K.T., and Lloyd, J.R., 1987b. A Numerical Study of Three-Dimensional Laminar Natural Convection in a Horizontal Cylinder with Differentially-Heated End Walls at High Rayleigh Numbers. Proceedings of the Symposium on Heat and Mass Transfer Honoring Professor B. T. Chao, University of Illinois, Urbana, IL, pp. 153-195.

Yang, H.Q., Yang, K.T., and Lloyd, J.R., 1988. Finite-Difference Calculations of Three-Dimensional Laminar Buoyant Flows Based on Curvilinear Non-Orthogonal Coordinates, Proceedings of the International Conference on Computational Engineering Science, Springer International, pp. 55.III. 1-55. III.4.

INITIAL DISTRIBUTION LIST

		No. Copies
1.	Library, Code 0142 Naval Postgraduate School Monterey, CA 93943-5100	2
2.	Research Administration, Code 012 Naval Postgraduate School Monterey, Ca 93943-5100	1
3.	Chairman, Code 69 Department of Mechanical Engineering Naval Postgraduate School Monterey, CA 93943-5100	2
4.	Professor M.D. Kelleher, Code 69Kk Department of Mechanical Engineering Naval Postgraduate School Monterey, CA 93943-5100	10
5.	Lt. Janet Raycraft SUPSHIP Sturgeon Bay Sturgeon Bay, WI	2
6.	Professor K.T. Young Department of Aerospace and Mechanical Engineering University of Notre Dame Notre Dame, IN 46556	6
7.	Dr. Patricia Tatem, Code 6183 Naval Research Laboratory Washington, DC 20375	4
8.	Mr. James Gagorik Office of Naval Technology 500 N. Quincy Arlington, VA 22217	1
9.	Capt. Raymond Michelini, Code 56Y Naval Sea Systems Command Washington, DC 20362	2
10.	Mr. Arthur Spero, Code 55X Naval Sea Systems Command Washington, DC 20362	2
11.	Defense Technical Information Center Cameron Station Alexanderia, VA 22304-6145	2